Characterizing climate and Mississippi river input into the Gulf of Mexico during two Pliocene glacials

Master thesis

Utrecht University

Faculty of Geosciences

Department Earth Sciences

Master Earth, Life and Climate

Magali Bouquet

July 2019

45 ECTS

Supervisors:

Dr. Francien Peterse (Organic Geochemistry)

Dr. Francesca Sangiorgi (Marine Palynology)

Table of contents

List of figures

Abstract

Last time in Earth's history when atmospheric CO_2 was comparable or slightly higher than at present was during the early Late Pliocene (3.6 to 3.0 Ma). During this generally warm period, one intense glaciation occurred (known as M2, lasting between 3.312 and 3.264 Ma), followed by the mid-Piacenzian Warm Period. The transition from M2 to the mid-Piacenzian Warm Period is often seen as an analogue for the climate of our (near) future. The end of the mid-Piacenzian Warm Period started with the less intense G20 glacial (3.025 Ma), followed by other less intense glacials. This study focuses on a marine sediment record from ODP Site 625 taken offshore the Mississippi delta, which is, therefore, expected to contain both marine and terrestrial material. The aim of this study is to reconstruct the terrestrial (hydro)climate and associated Mississippi input into the Gulf of Mexico (GoM) as well as the oceanographic changes in the Gulf of Mexico during two glacial periods: M2 and the less intense G20 using a multi-proxy approach of both lipid biomarkers and palynology. The absence of plant- and soil-derived lipid biomarkers and pollen in the sediments indicate that terrestrial material discharged to the ocean by the Mississippi did not reach the site location during the studied intervals. On the other hand, marine lipid biomarkers and dinoflagellate cysts reveal a strong influence of the Loop Current during the interval preceding M2, transporting warm and salty Caribbean waters into the Gulf of Mexico. During the cold M2 interval, TEX_{86} sea surface temperatures dropped from 22.7°C to 20.6°C and U^{k}_{37} sea surface temperatures from 27.2°C to 26.2°C. During the temperature drop, salinity and stratification of the water column increased, eventually resulting in hyperstratification, as indicated by the presence of *P. zoharyi.* Hyperstratification still lasted into the following mid-Pliocene Warm Period, at least until 3.247 Ma. Eventually, the change in dinocyst composition shows that Caribbean waters entered the northern Gulf of Mexico again after 3.247 Ma. At the onset of the G20, sea surface temperatures based on TEX_{86} dropped from 23.2°C to 18.8°C and periods of hyperstratification occurred, although less intense than during M2.

1. Introduction

Global climate is rapidly warming. At the end of the 21st century, global mean surface temperatures between 0.3°C to 1.7°C and 2.6°C to 4.8°C higher than present day are predicted, depending on the CO_2 emissions scenario (IPCC, 2014). This temperature increase will have an effect on vegetation and biome distributions, which in turn will influence climate feedback systems (Salzmann et al., 2008). The most recent period where CO_2 levels were higher than present-day was during the early Late Pliocene (early Piacenzian), lasting from 3.6 to 3.0 Ma. Especially the period from 3.3 to 3.0 Ma, the mid-Piacenzian Warm Period (mPWP), is intensively studied. During this period, atmospheric CO_2 levels were between 330 and 400 ppm, which is comparable to modern day values (Seki et al., 2010) while global temperatures were around 2.7°C to 4.0°C higher than today (Haywood et al., 2016). Because of those similar CO_2 levels and higher temperatures, the Late Pliocene has been widely studied to establish the long-term effect of increased CO_2 levels in the atmosphere (Dolan et al., 2015) on climate and predict its near future trend.

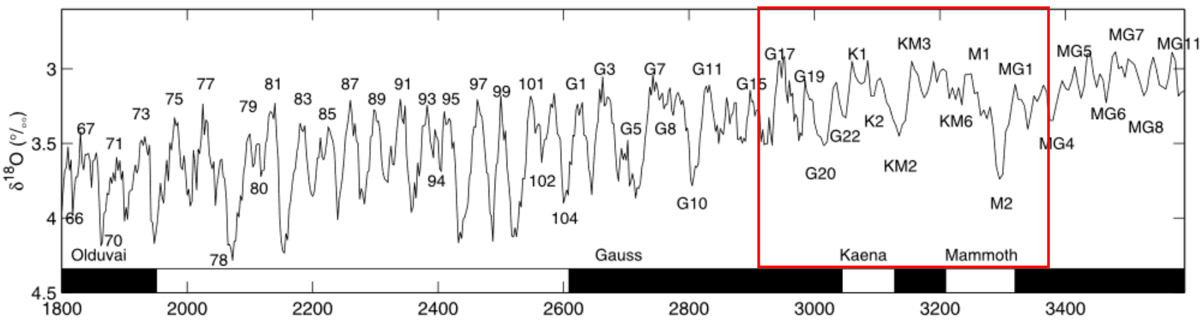

Figure 1: The $\delta^{18}O$ benthic stack with the glacials (even numbers) and interglacials (odd numbers) indicated (Lisiecki & Raymo, 2005). The period of interest is indicated with a red box.

Approximately 3.3 million years ago, this warm global climate was interrupted by a short, intense global glaciation (Lisiecki & Raymo, 2005). This glaciation, indicated as M2 (3.312 to 3.264 Ma, figure 1), started as a low amplitude glaciation that has been considered as a ‘failed attempt’ of the earth to switch to the glacial-interglacial mode that characterized the Pleistocene. However, between 3.305 and 3.285 Ma, this glaciation intensified and reached values similar of early Quaternary glaciations (De Schepper et al., 2013). During M2, global temperatures were comparable to today’s temperatures, although both Northern as Southern Hemisphere ice sheets were likely slightly larger. Because of those characteristics, the transition from M2 to the mPWP can provide valuable insights into future climate, as it may be comparable to the shift the climate system has undergone since the last glacial (De Schepper et al., 2013).

Compared to present day, the global terrestrial climate during the Piacenzian was warmer and wetter, which caused a northward shift of the temperate and boreal vegetation zones. Furthermore, deserts were more reduced while tropical savannas and forests expanded. The wetter climate also supported the formation of megalakes like Lake Zaire and Lake Chad (Dowsett et al., 2016). However, the terrestrial surface air temperature reconstructions have a number of uncertainties. The main cause of this is a lack of suitable climate archives and methods to generate high resolution paleoclimate records. Especially central North America, South America and northwestern Africa have a low data coverage. Furthermore, uncertainty is caused by the resolution of the individual records and the insufficient age control (Dowsett et al., 2016).

As there is a lack of terrestrial climate archives, marine sediments close to large river mouths can be used to make terrestrial climate reconstructions. Large rivers transport terrestrial material to the location where the sediments are deposited. Furthermore, marine sediments also contain (molecular) fossils of marine organisms .Hence, continental margin sediments contain an archive of both terrestrial and marine components that allow to study environmental changes through time. Furthermore, when benthic foraminifera are present in the marine sediments, and the sediments have a high sedimentation rate, the oxygen isotopes ($\delta^{18}O$) on the foraminiferal shells can be used to construct an age model by matching the obtained $\delta^{18}O$ record with that of the global compilation (L&R, 2005).

Lipid biomarkers are molecular fossils that can be used as organic geochemical climate proxies. Based on their occurrence, or variations in their molecular structure, and/or their isotopic composition, various climate parameters, such as temperature, salinity and sea-ice can be reconstructed (Eglinton & Calvin, 1967). The lipid biomarker proxies that will be studied here are plant leaf waxes for terrestrial input and vegetation changes, alkenones for sea surface temperature (SST) reconstruction (U^{k}_{37}), isoprenoidal glycerol dialkyl glycerol tetraether (GDGT) membrane lipids for the reconstruction of SST (TEX_{86}) and fluvially discharged soil input (BIT index) and long chain diols (%C_{32} diols) for fresh water input.

Higher plant leaves have a cuticular wax layer, which is composed of odd numbered long-chain n-alkanes (Eglinton and Hamilton, 1967) to protect the leaves against uncontrolled water loss (Sachse et al., 2012). Changes in vegetation type associated to changing hydrological conditions will be assessed using the average chain length of the long-chain n-alkanes. Shorter chain lengths (C_{27} and C_{29}) indicate more trees and shrubs, whereas longer chain lengths (C_{31} and C_{33}) indicate more grasses (Castañeda et al., 2016).

Alkenones are produced by haptophyte algae and have various amounts of double bonds. The haptophyte algae adapt their degree of unsaturation according to changes in sea surface temperatures. The degree of unsaturation is captured in the U^{k}_{37}, which can consequently be translated into sea surface temperatures. U^{k}_{37} is based on the ratio between the concentrations of the di- and tri-unsaturated C_{37} alkenones (Prahl and Wakeham, 1987; Müller et al 1998).

Isoprenoid GDGTs are formed as the membrane lipids of marine Thaumarchaeota. Those GDGTs contain cyclopentane rings, which increase in number when water temperatures increase (Schouten et al., 2002). TEX_{86} (TetraEther index of tetraethers consisting of 86 carbon atoms) is a SST proxy based on the relative abundances of isoprenoid GDGDs containing 1-3 cyclopentane moieties (Kim et al., 2010). Soil bacteria produce branched GDGTs, so with the ratio between the isoprenoid and branched GDGTs, the relative input of terrestrial material into a marine system can be determined, quantified in the Branched and Isoprenoid Tetraether (BIT) index (Hopmans et al., 2004).

Long chain diols can be used as a proxy for riverine input in shelf seas. Long chain diols are generally abundant in the marine environment, however, C_{32} 1,15-diols are only produced in fresh water environments, and discharged to the ocean by rivers. Hence, the relative abundance of the C_{32} 1,15-diols can be used as a measure for fresh (melt)water input (Lattaud et al., 2017).

Marine and terrestrial palynology studies dinoflagellate cysts (dinocysts) and pollen and spores, respectively. These methods are widely used to achieve climate and environmental reconstructions of land and sea conditions at the same time (Reid & Harland, 1977). Dinocysts are resting cysts of dinoflagellates, which are mostly single-celled eukaryotic plankton (Wall & Dale, 1968). Dinoflagellate assemblages are controlled by different environmental parameters such as temperature, productivity, salinity, sea-ice cover, seasonality and sea-level. As the dinocyst assemblages are influenced by the water's biological, physical, chemical and oceanographic conditions, they can be used as a proxy for paleoenvironmental changes in the upper water column (Zonneveld et al., 2013).

Hence, in order to extend the spatial resolution of late Pliocene terrestrial climate reconstructions, this research focuses on a sediment record from the Northern Gulf of Mexico, close to the present Mississippi delta. Due to its location close to the coast, the record is expected to contain both a marine and terrestrial signal. We here aim to reconstruct the (hydro)climate and associated Mississippi input into the Gulf of Mexico (hereafter GoM) as well as the oceanographic changes in the GoM during two glacial periods: M2 (age) and the less intense G20 (3.025 Ma, Figure 1) using a multi-proxy approach of both lipid biomarkers and palynology.

2. Material and Methods

2.1 Study site and oceanographic features

Ocean Drilling Program (ODP) Site 625 was cored in the north-eastern GoM in 1985 as part of Leg 100. The cores from Hole 625B were retrieved from the western Florida continental slope, at a water depth of 889 meter and approximately 200 km from the present Mississippi delta, as is shown in figure 2 (Limoges et al., 2014). For this study, samples from a depth of 134.1 to 148.28 meter below sea floor (mbsf) were used. The age model for Hole ODP 625B is taken from Van der Weijst & Dearing Crampton-Flood (in prep). They measured the oxygen isotopic composition of benthic foraminifera, which they wiggle-matched to the benthic stack of Lisiecki & Raymo (2005). The ages corresponding to the depths used in this study are 2.929 Ma to 3.400 Ma. In the resulting $\delta^{18}O$ record, the M2 and G20 are identified, and there appear to be no hiatuses.

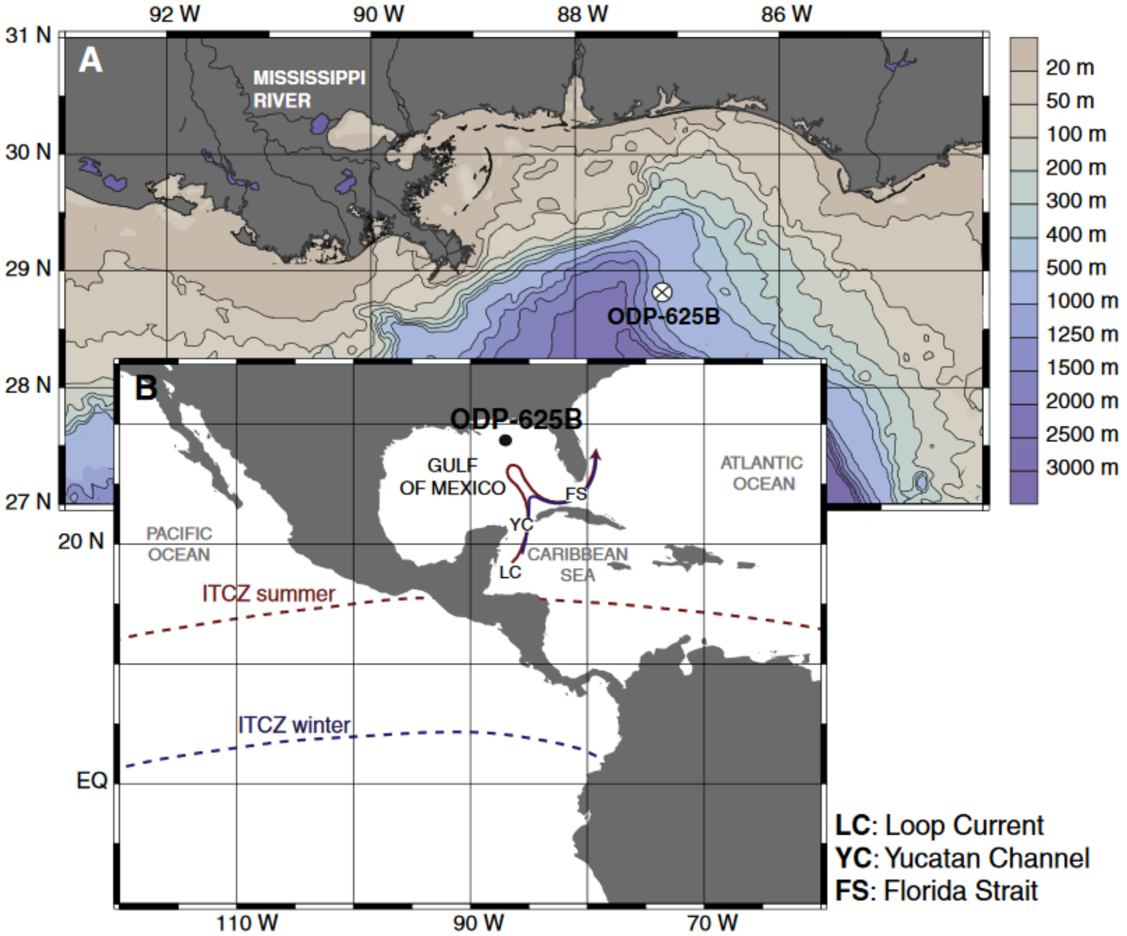

Figure 2: A) Location of ODP 625B. B) Location of the Loop Current (LC) which enters the GoM through the Yucatán Channel (YC) and exits through the Florida Strait (FS) (Limoges et al., 2014).

An important oceanographic feature in the GoM is the Loop Current (LC), which is the dominant surface current in the GoM. The LC enters the GoM through the Yucatán channel, bringing warm and salty water from the Caribbean Sea. The LC then moves northeast, and exists the GoM via the Florida Strait (Figure 2). The northward extension of the LC depends on the Intertropical Convergence Zone (ITCZ). When the ITCZ migrates north during boreal summer, the LC penetrates further north into the GoM influencing the temperature and salinity of the entire basin (Nürnberg et al., 2008). The LC runs from west to east in the Gulf of Mexico, so although the present-day Mississippi discharge is more to the west than the site 625 location, it is expected that currents transported material to the site location so the records likely contain material transported by the Mississippi. Another reason to expect terrestrial material in the records is the presence of terrestrial material in the Pleistocene section of these cores (Romanin, 2013, unpublished).

2.2 Biomarker analysis

A total of 136 samples were selected for biomarker analysis. The samples were freeze-dried, ground with mortar and pestle, and 5 gram of the samples was extracted using an accelerated solvent extractor (ASE) generating a total lipid extract (TLE). By using a small column with activated aluminium oxide, the TLE was separated into three different fractions: an apolar, a ketone and a polar fraction using hexane:dicholoromethane (DCM) 9:1, hexane:DCM 1:1 and DCM:methanol 1:1 respectively.

The apolar fraction, containing the long chain n-alkanes, was dissolved in hexane and analysed on a Gas Chromatograph (GC) coupled to a flame ionisation detector (GC-FID, Hewlett Packard 6890 series). Samples were injected on-column, with helium as a carrier gas at a flow rate of 2 ml/min. The oven temperature program was as follows: 130°C at 20 min, then to 320°C at a rate of 4°C/min, and held isothermal for 10 min. Peak areas of the C_{27}, C_{29}, C_{31} and C_{33} alkanes were determined to calculate the average chain length (ACL) following Poynter et al. (1989):

$$ACL = \frac{27\mathrm{C}_{27} + 29C_{29} + 31\mathrm{C}_{31} + 33\mathrm{C}_{33}}{(\mathrm{C}_{27} + C_{29} + \mathrm{C}_{31} + \mathrm{C}_{33})}$$

The ketone fraction, containing the alkenones, was dissolved in hexane and analysed on the GC-FID with the same settings as used for the apolar fraction. The peak areas of the $C_{37:2}$ and $C_{37:3}$ alkenones were determined to calculate the U^{k}_{37} and SST using the following equations (Prahl & Wakeman, 1987):

$$U^{k}_{37} = \frac{\mathrm{C}_{37:2}}{(C_{37:3} + \mathrm{C}_{37:2})}$$

$$SST = \frac{U^{k}_{37} - 0.043}{0.033}$$

For the analysis of the GDGTs, an known amount of internal C_{46} standard was added to the polar fraction (Huguet et al., 2006). The fractions were then dissolved in hexane:isopropanol 99:1 and filtered using a 0.45 µm PTFE filter. The samples were analysed according to Hopmans et al. (2016) using an Agilent 1260 high performance liquid chromatography-mass spectrometry (HPLC-MS). Separation of the GDGDs occurred by using two silica Waters UHPLC HEB Hilic columns (1.7 µm 2.1 mm x 150 mm) at 30°C. The used flow rate is 0.2 ml/min, starting with 82% hexane and 18% hexane:isopropanol 9:1 for 25 min with a linear gradient to 70% hexane and 30% hexane:isopropanol 9:1 for 25 min (Hopmans et al., 2016). To calculate SSTs using TEX_{86}, the formulas of Kim et al. (2010) are used:

$$TEX^{H}_{86} = \frac{(\mathrm{GDGT2} + \mathrm{GDGT3} + \mathrm{Cren'})}{(\mathrm{GDGT1} + \mathrm{GDGT2} + \mathrm{GDGT3} + \mathrm{Cren'})}$$

$$SST = 68.4 * (LOG(TEX^{H}_{86})) + 38.6$$

To calculate the BIT index as a proxy for the relative abundance of terrestrial organic matter the formula of Hopmans et al. (2004) is used:

$$BIT\ index = \frac{(\mathrm{GDGT1} + \mathrm{GDGT2} + \mathrm{GDGT3})}{(\mathrm{Cren} + \mathrm{GDGT1} + \mathrm{GDGT2} + \mathrm{GDGT3})}$$

After GDGT analysis, a selection of the polar fractions was derivatized by silylation using BSTFA and pyridine. After adding bis(trimethylsilyl)trifluoroacetamide (BSTFA) and pyridine, the samples were heated at 60°C for 20 min. Then ethylacetate was added and the samples were analysed by a GC-MS on SIM mode. The diols used for analysation are C_{32} 1,15, C_{30} 1,15, C_{30} 1,13 and C_{28} 1,13. The river input can be calculated with the following equation of Lattaud et al. (2017), where a C_{32} 1,15 diol percentage lower than 10% represents open oceans:

$$\%\ C_{32}1{,}15 = \frac{\mathrm{AC}_{32}1{,}15}{(\mathrm{C}_{32}1{,}15 +\ \mathrm{C}_{30}1{,}15 +\ \mathrm{C}_{28}1{,}13 +\ \mathrm{C}_{30}1{,}13)} * 100$$

2.3 Palynology

A total of 35 samples was selected for palynological analysis. For each sample, 10 grams of freeze-dried sediment was ground and a *Lycopodium clavatum* tablet containing 9666 spores was added to be able to later determine the absolute amounts of pollen, spores and dinocysts. The samples were subsequently treated with hydrochloric acid (10% and 30%) to dissolve the calcium carbonates, and then with hydrofluoric acid (40%) to dissolve the silicates. The residue was sieved at 10 µm, during which an ultrasonic bath was used to remove the fine fraction. Finally, the samples were mixed with glycerine jelly, mounted on a microscope plate and counted using a microscope with 400x magnification. For each slide, at least 200 dinocysts were counted.

To make an environmental reconstruction based on the dinocysts, the environmental preferences of each dinocysts as summarized by Zonneveld et al. (2013) are used. The most common species with clear environmental preferences in the present day GoM are *Polysphaeridium zoharyi, Operculodinium centrocarpum, Operculodinium israelianum* and *Impagidinium spp.* (Limoges et al., 2013). The environmental preferences for those species are, respectively, coastal with high upper water salinities, opportunistic, subtropical to equatorial with high upper water salinities and open ocean. Dinoflagellates can have three different feeding strategies: autotrophic, mixotrophic and heterotrophic. Autotrophic species are capable of photosynthesis, heterotrophic species feed on prey and mixotrophic species are capable of both. Heterotrophic species dominate assemblages in productive areas (Pospelova et al., 2006). During this study, all heterotrophic species are grouped together as proxy/indication for productivity. The other mentioned species are autotrophic species.

Furthermore, different calculations are used:

$$Rel.abundance\ species\ X = \frac{Species\ X}{\mathrm{Total\ dinocysts}} * 100$$

$$\mathrm{Abs.abundance\ species\ X} = \frac{\mathrm{Species\ X} * \mathrm{Total}\ Lycopodium}{Lycopodium\ counted}$$

$$Dinocysts\ per\ gram\ sediment = \frac{\text{Total dinocysts}}{\text{Gram used sediment} * Lycopodium/\text{Total } Lycopodium}$$

The ratio between the open water and oligotrophic species *Impagidinium spp.* (I) and the coastal, high salinity and stratification species *P. zoharyi* (P) can be used as a proxy for proximity of the site to the coast during the Pleistocene at site ODP 625B (Romanin, 2013, unpublised). This ratio is based on the present day distribution of the dinocysts and calculated by using the formula:

P. zoharyi over *Impagidinium* spp. ratio = (P/P+I)*100

The pollen and spores are not identified but used to calculate the pollen over dinocyst ratio as used by Donders et al. (2009) using the total abundances of the pollen (P), excluding the bisaccata taxa, and dinocysts (D):

Pollen over dinocyst ratio = (P/D+P)*100

As pollen and spores originate from land, and dinocysts from oceans, the pollen over dinocyst ratio can used as an indicator of the origin of the organic flux (De Vernal & Giroux, 1991).

3. Results

3.1 Input of terrestrial material to ODP Site 625

Several proxies have been used to evaluate the terrestrial input to the site, and all proxies show that the sediments are depleted in terrestrial material throughout the whole studied interval. The amounts of diols and long chain n-alkanes are around or below detection limit, and can thus not be quantified. The BIT index throughout the whole record varies between 0.02 and 0.06 (figure 3). The pollen over dinocyst ratio is between 0 and 15.6% throughout the record except for two slight increases in the amount of pollen and spores at 3.392 Ma and 2.997 Ma, which results in a decrease in the pollen over dinocyst ratio to 15.6% and 11.4% respectively (figure 3).

It is remarkable that even during the cold M2 event, no terrestrial markers or an increased BIT index are found while during the M2 a sea level drop is expected, bringing the Mississippi river mouth closer to the site OPD 625B.

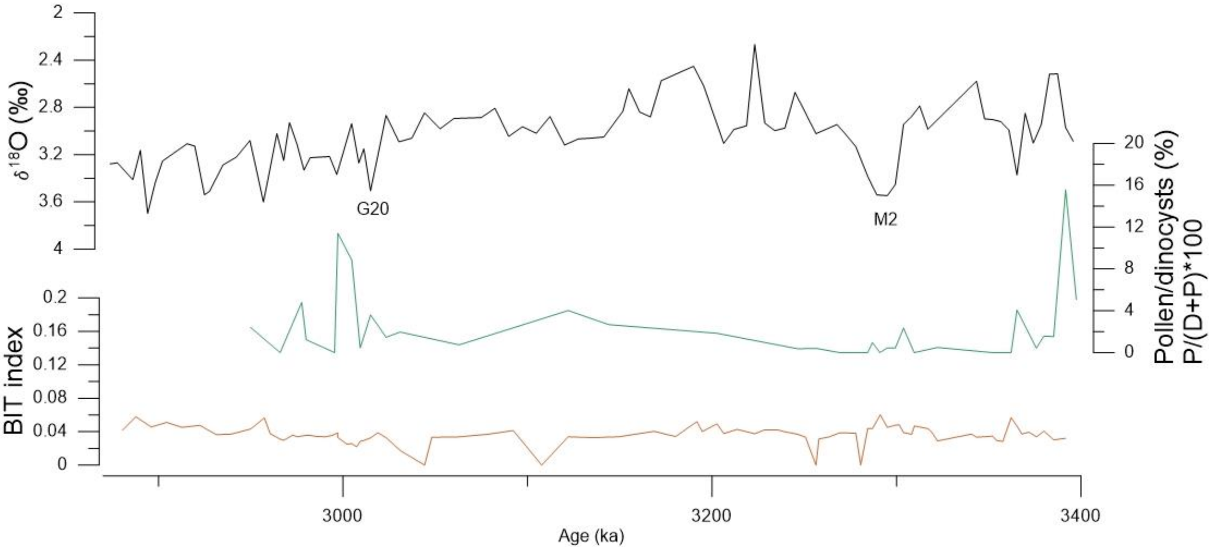

Figure 3: $\delta^{18}O$ record, pollen over dinocyst ratio and BIT index of ODP 625B.

3.2 Marine biomarkers

As opposed to the terrestrial biomarkers, alkenones and GDGTs are present throughout the whole record. The U^{k}_{37} values are between 0.92 and 0.97, which is close to saturation, and correspond to a temperature range of 26-28°C. The TEX_{86} values are between 0.54-0.63, corresponding to a temperature range of 19-25°C. A remarkable observation is the large variation in the TEX_{86} record with regard to the U^{k}_{37} record: the amplitude of variation in the TEX_{86}-derived SST record is higher than that in the SST record based on the U^{k}_{37}, as can be seen in figure 4.

The U^{k}_{37} temperatures are higher than the TEX_{86} temperatures, although both SST records follow the same trend, and also correspond to the $\delta^{18}O$ record as is visible in figure 4. During the oldest studied interval, from 3.398 Ma to 3.376 Ma, the SSTs are between 23.5°C and 25.1°C based on TEX_{86} and 26.8°C and 27.6°C based on $U^{k}_{37.}$ Both records show a drop in temperature with lowest temperatures at 3.365 Ma where the U^{k}_{37} SSTs are 26.6°C and the TEX_{86} SSTs 21.4°C.

This colder interval is followed by a short warm period from 3.362 Ma to 3.301 Ma before the SSTs drop again, marking the start of M2. The cold M2 event (3.301 to 3.278 Ma) lasts longer than the previous cold event, and has the coldest SSTs at 3.291 Ma. Here again, the U^{k}_{37} drop is more gradual and less intense than the TEX_{86} drop. U^{k}_{37} drops from 27.2°C to 26.2°C whereas TEX_{86} drops from 22.7°C to 20.6°C.

The M2 is succeeded by an extended warm interval from 3.278 Ma to 3.023 Ma with high SSTs, the mPWP. The U^{k}_{37} SSTs have an average temperature of 27.6°C, while the TEX_{86} SSTs have an average temperature of 23.1°C. This period ends at 3.023 Ma with a SST drop, the start of G20. This SST drop is especially visible in the TEX_{86} record which drops from 23.2°C to 18.8°C whereas the U^{k}_{37} record drops from 27.8°C to 27.2°C.

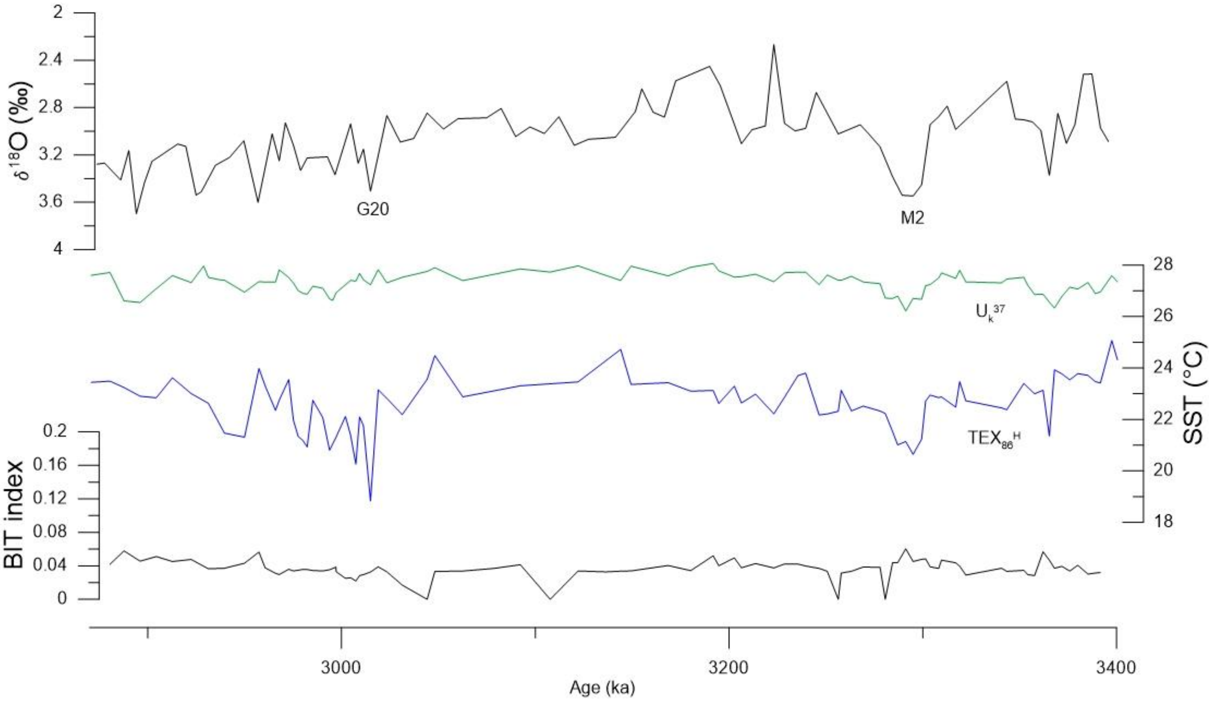

Figure 4: The δ18O, Uk37, TEX86 and BIT index during the Late Pliocene of ODP site 625B.

3.3 Dinoflagellates

The dinoflagellate cysts are very well preserved and their concentrations vary between 2397-54174 dinocysts/gram dry sediment (Appendix 3). Phototrophic species dominate over heterotrophic species, which reaches a maximum total relative abundance of 14% throughout the whole interval. The phototrophic species assemblages are diverse. The species that reaches the highest relative occurrence is *Polysphaeridium zoharyi* (1-95%). Other common species are *Spiniferites* spp (3-39%), *Operculodinium centrocarpum* (0-31%), *Pentapharsodinium dalei* (0-21%), *Spiniferites ramosus* (0-20%) and *Operculodinium israelianum* (0-19%). Species with minor abundances are *Spiniferites mirabilis* and *hyperacanthus* (0-11%), *Impagidinium* spp. (0-11%), *Lingulodinium machaerophorum* (0-15%), *Nematosphaeropsis labyrinthus* (0-5%) and *Bitectatodinium tepikiense* (0-1%). *Spiniferites spp.* mostly consists of *S. ramosus* and *S. mirabilis/hyperacanthus,* but as those species do not have clear environmental preferences, all *Spiniferites* are taken together.

The oldest part of the studied record, from 3.398 Ma to 3.376 Ma, mostly contains *Spiniferites* spp*., Impagidinium* spp*, O. centrocarpum*, O*. israelianum* and *P*. *dalei*. At 3.365 Ma the assemblage changes, an increase of *O. centrocarpum*, *L*. *machaerophorum* and *P*. *zoharyi* occurs while *Impagidinium* spp*, O*. *israelianum* and *P*. *dalei* decrease. Also *B*. *tepikiense* appears, as is visible in figure 5, although in very low relative abundances (1%). After this short increase of *O. centrocarpum* and *L*. *machaerophorum* at 3.365 Ma, they decrease again while *P*. *zoharyi* increases further, reaching relative abundances of up to 64% at 3.352 Ma. At 3.303 Ma *P*. *zoharyi* decreases to 22% before increasing to very high relative abundances of up to 95% at 3.284 Ma. During the short decrease of *P*. *zoharyi* at 3.303 Ma, *O*. *israelianum* and *O*. *centrocarpum* increase.

P. *zoharyi* relative abundance remains high, between 67% and 95% until ~3.246 Ma. Between 3.246 Ma and 3.031 Ma, only four datapoints exist so it is impossible to draw a clear trend. However, the assemblages have changed as *P*. *zoharyi* has low abundances of 5% to 16%, with one exception of 61% at 3.122 Ma. During this interval, *O*. *centrocarpum* and *L*. *machaerophorum* are the common species.

At 3.015 Ma the dinocyst assemblage changes, an increase of *O*. *centrocarpum* to 38% is followed by an increase in *L*. *machaerophorum* from 9% to 15% at 3.009 Ma. From 3.005 Ma *P*. *zoharyi* starts to increase again, reaching values of up to 80% at 2.996 Ma. After this period of high *P*. *zoharyi* abundances, it decreases but is still higher than during the period before, around 20-40% and remains a very abundant species.

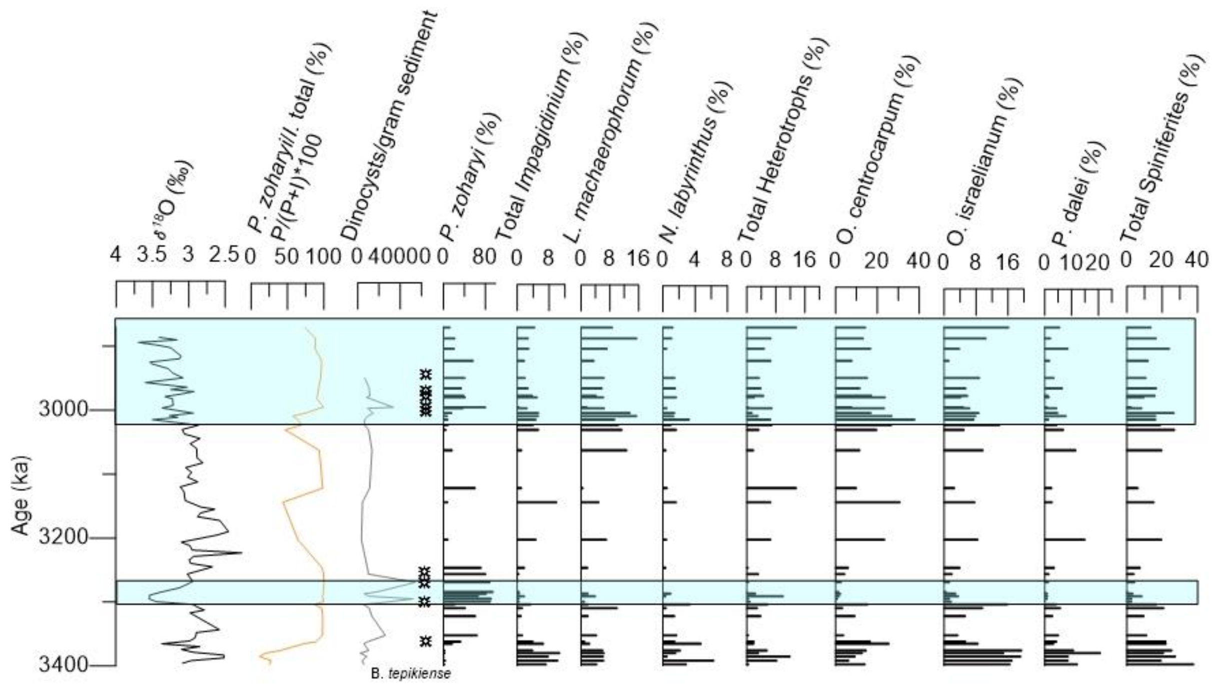

Figure 5: The δ18O record, P. zoharyi over Impagidinium spp. ratio, amount of dinocysts/gram sediment and the relative abundances of the most abundant dinoflagellate cysts.

Table 1: Autotrophic dinocyst species distribution based on Zonneveld et al. (2013).

Species	**Environment**
Polysphaeridium zoharyi	Coastal species, characteristic for subtropical to equatorial regions. Can reach high abundances in areas where high upper water salinities exist. Euryhaline species, tolerates very high and very low salinity
Operculodinium centrocarpum	Cosmopolitan species, occurs from polar to equatorial regions and coastal to open ocean. It is an opportunist.
Pentapharsodinium dalei	Cosmopolitan species, occurs from polar to equatorial regions and coastal to open ocean.
Spiniferites ramosus	Cosmopolitan species, occurs in subpolar to equatorial regions.
Operculodinium israelianum	Subtropical to equatorial species. Reaches high abundances in nearshore sites and in areas with high upper water salinities.
Spiniferites mirabilis/hyperacanthus	Temperate to equatorial distribution, coastal as well as open ocean.
Impagidinium spp.	Open ocean
Lingulodinium machaerophorum	Temperate to equatorial environments. Reaches high abundances near upwelling areas and river mouths and during times with upper water stratification.
Nematosphaeropsis labyrinthus	Cosmopolitan species, occurs from arctic to equatorial, fully marine environments.
Bitectatodinium tepikiense	Subpolar to temperate regions.

4. Discussion

4.1 Terrestrial biomarkers

The presence and concentration of terrestrial biomarkers is limited throughout the entire studied interval. Low pollen and alkane abundances indicate little terrestrial input. This is supported by the low BIT index (<0.06). Furthermore, the absence of C_{32} diols in the record indicates that fresh water discharge by rivers was either limited, or did not reach site ODP 625B. The latter scenario could be explained by changes in sea level, and/or the position of the river mouth during the Piacenzian. Sea level estimates range from no change at all up to a sea level rise of 50 meters (Dolan et al., 2016). However, during the cold M2 interval, the sea level drop is estimated at 10 m±10-15 m (Naish & Wilson, 2008), 40 m±10 m (Miller et al., 2012) or up to 65 m±15-25 m (Dwyer & Chandler, 2008) below present sea level as summarized by De Schepper et al. (2013) in figure 6. This is a large uncertainty and would have different implications for the paleoshoreline, as can be seen in figure 6 which shows different paleoshorelines for different sea level drops. In case of a 80-100 meter sea level drop, the shoreline would be much closer to the site, probably resulting in more terrestrial input. As there is no terrestrial input, it seems unlikely that the sea level drop was that large.

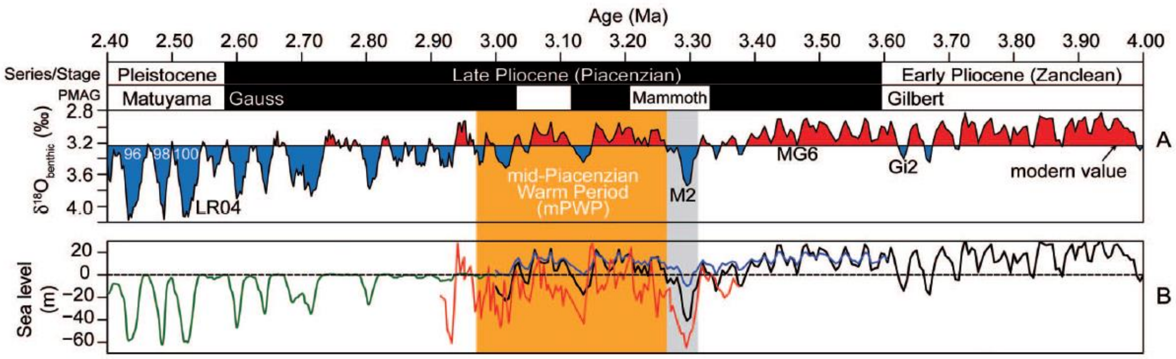

Figure 6: A) The δ18O record based on the global benthic stack of Lisiecki & Raymo (2005). B) Sea level estimates of the Pliocene. Blue = Naish & Wilson (2008), Black = Miller et al. (2012) and Red = Dwyer & Chandler (2008). Figure after De Schepper et al. (2013).

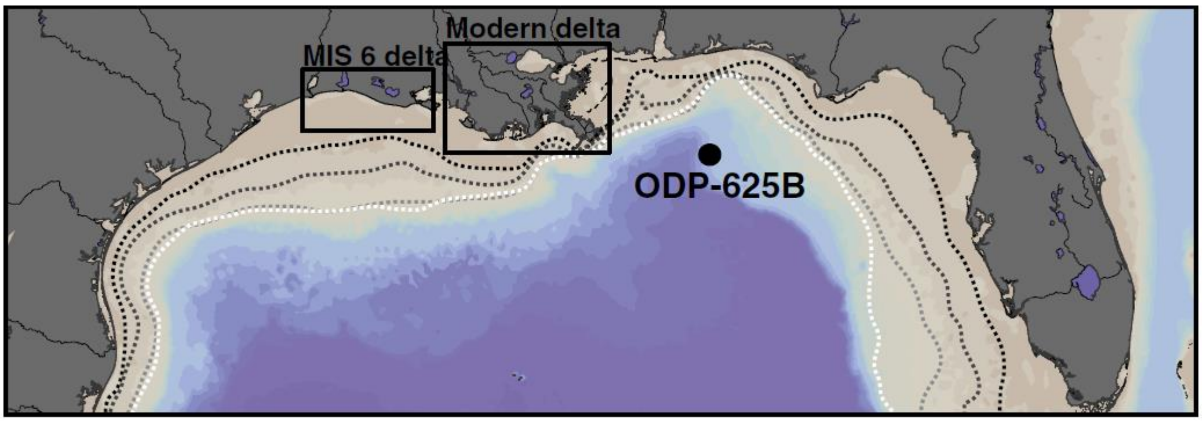

Figure 7: Different paleoshorelines for different sea level drops based on model simulations. White=100 mbsl, light grey=80 mbsl, dark grey=40 mbsl and black=20 mbsl (Limoges et al., 2014).

During interglacials and interstadials of the last 400 kyr, most of the Mississippi discharge flowed westward. As the ITCZ had a more northward position and the LC was strong and flowing in northward direction, the conditions in the northeastern GoM became similar to the conditions in the western Caribbean (Nürnberg et al., 2008). A strong northward flowing LC during the Pliocene pushing the Mississippi discharge to the west can also explain the lack of terrestrial material in the records. However, at 2.515 Ma, pollen were abundant at ODP site

625B (Romanin, 2013), indicating terrestrial influence during the Pleistocene. From this can be concluded that the Mississippi changed its course between 2.950 Ma and 2.515 Ma, possibly in combination with sea level lowering.

As there appears to be almost no terrestrial input to ODP site 625B during the Pliocene, the main focus of this thesis is, therefore, on the reconstruction of past climatic changes in the marine environment.

4.2 Interpretation of the TEX_{86} and U^{k}_{37} records

Although the TEX_{86} and U^{k}_{37} records show largely the same trends, the U^{k}_{37} record is much more stable than the TEX_{86} record, which shows higher variability. During the Late Pliocene, average SSTs based on TEX_{86} is 22.7°C with a maximum amplitude of 6.2°C, while the average SST based on U^{k}_{37} is 27.3°C, with a maximum amplitude of 1.8°C. The current mean annual sea-surface temperature is 25.9°C, with a large seasonal amplitude of 8.5°C (Limoges et al., 2014). U^{k}_{37} and TEX_{86} are both SST proxies. However, seasonality, depth distribution and diagenesis likely influence their downcore SST variability (Richey & Tierney, 2016).

Seasonality can explain (part of) the difference between the TEX_{86} and U^{k}_{37} records. In the global ocean, alkenone production is spring-summer weighted but, at least in the modern day GoM, the highest primary production of both alkenones and isoGDGTs occurs in winter. This is a result of the higher wind driven mixing of the upper water column during this season (Richey & Tierney, 2016). However, alkenone production during the Late Pliocene likely occurred during summer as the reconstructed U^{k}_{37} temperatures are on average 27.3°C and correspond with the modelled August SSTs of 28°C (Dowsett et al., 2009), as is visible in figure 8. It should be noted that the relation between U^{k}_{37} and SST becomes nonlinear when SSTs are between 24°C and 30°C (Richey & Tierney, 2016) and the U^{k}_{37} ratio becomes saturated when temperatures are 29°C or higher. So in very warm tropical waters, the usefulness of U^{k}_{37} is limited (Lawrence & Woodard, 2017). As the reconstructed U^{k}_{37} values in this study are almost saturated, part of the U^{k}_{37} SST variability can have been flattened out.

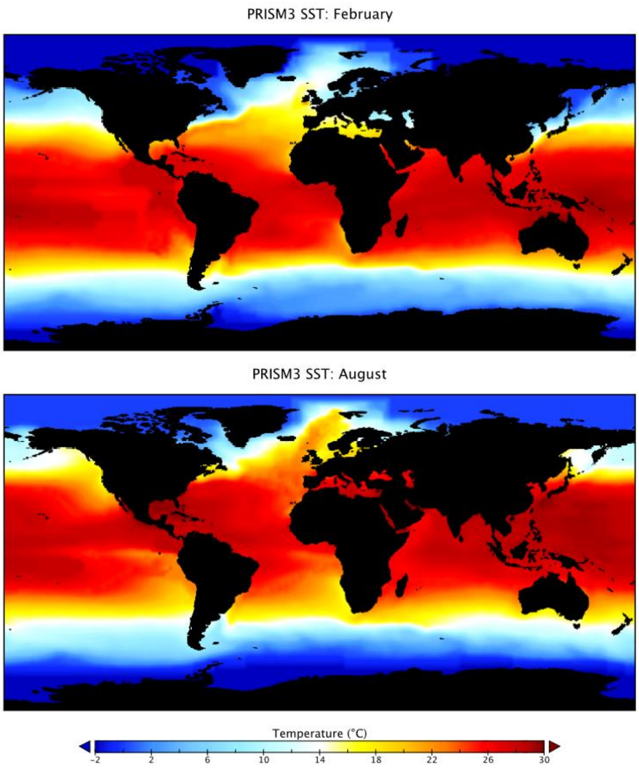

Figure 8: Modelled February and August SSTs by Dowsett et al. (2009).

The reconstructed TEX_{86} temperatures are on average 22.7°C and do not correspond with the modelled February temperatures of 20°C (Dowsett et al., 2009). This indicates that isoGDGT production occurred during a different season than summer or winter, or that the isoGDGT production is controlled by another factor.

Richey & Tierney (2016) compared the modern day alkenone and isoGDGT flux with core-top sediments in the northern Gulf of Mexico during a four year sampling interval. They found that the U^{k}_{37} record represents the near-surface mean annual temperatures, while the TEX_{86} records represents the mean annual subsurface temperatures from 0-200 m. As a result, the SSTs reconstructed with TEX_{86} lack seasonality (Richey & Tierney, 2016), which is also visible in figure 9.

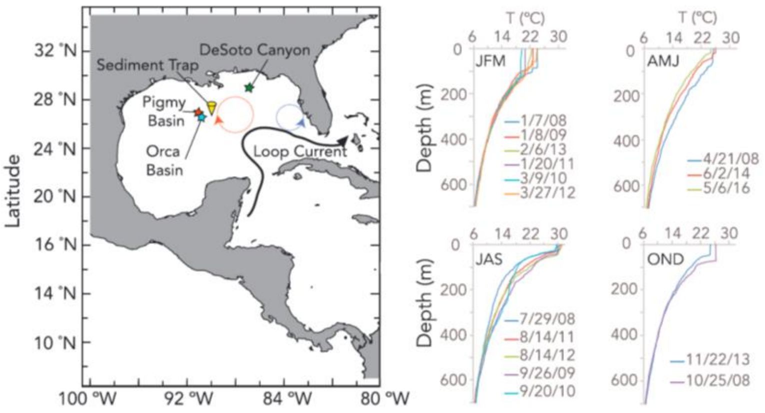

Figure 9: Vertical temperature profiles (Richey & Tierney, 2016).

Differences between TEX_{86} and U^{k}_{37} can also occur as a result of degradation. There are many marine bacteria that are able to degrade alkenones. Most of those bacteria do this nonselective (Zabeti et al., 2010). However, Zabeti et al. (2010) found one specific bacteria, the *Dietzia maris* sp., that does selectively degrade alkenones with a preference for the double bond at the 29th position. This selective degradation increased the U^{k}_{37} values with 0.05 to 0.10, leading to a SST increase of 1.5-3.0°C (Zabeti et al., 2010). Rickey and Tierney (2016) found a 1-2°C warm bias in the U^{k}_{37} SSTs in the modern day GoM as a result of selective degradation.

As the TEX_{86} SSTs do not match with reconstructed summer of winter temperatures, and Rickey an Tierney (2016) found that in the modern day GoM TEX_{86} reflects the mean annual subsurface (0-200 m) temperatures, the TEX_{86} SST record will be interpreted as subsurface sea temperatures. The reconstructed U^{k}_{37} SSTs correlate with the modelled summer SSTs of Dowsett et al. (2009). This in contrast with the modern day alkenone production in the GoM, which is winter weighted (Richey & Tierney, 2016). Rickey and Tierney (2016) also found that in the modern day GoM, U^{k}_{37} represents the near-surface temperatures. Therefore, the reconstructed U^{k}_{37} SSTs will be interpreted as near-surface sea temperatures.

4.3 Environmental reconstruction

Based on the $\delta^{18}O$ record of Van der Weijst (in prep), the record can be divided into four intervals, for which the SST records and palynology will be discussed:

1. The period towards M2 (3.400-3.312 Ma),
2. The M2 interval (3.312-3.264 Ma),
3. The mPWP (3.245-3.023 Ma)
4. The demise of the mPWP, starting with G20 (3.025-2.950 Ma)

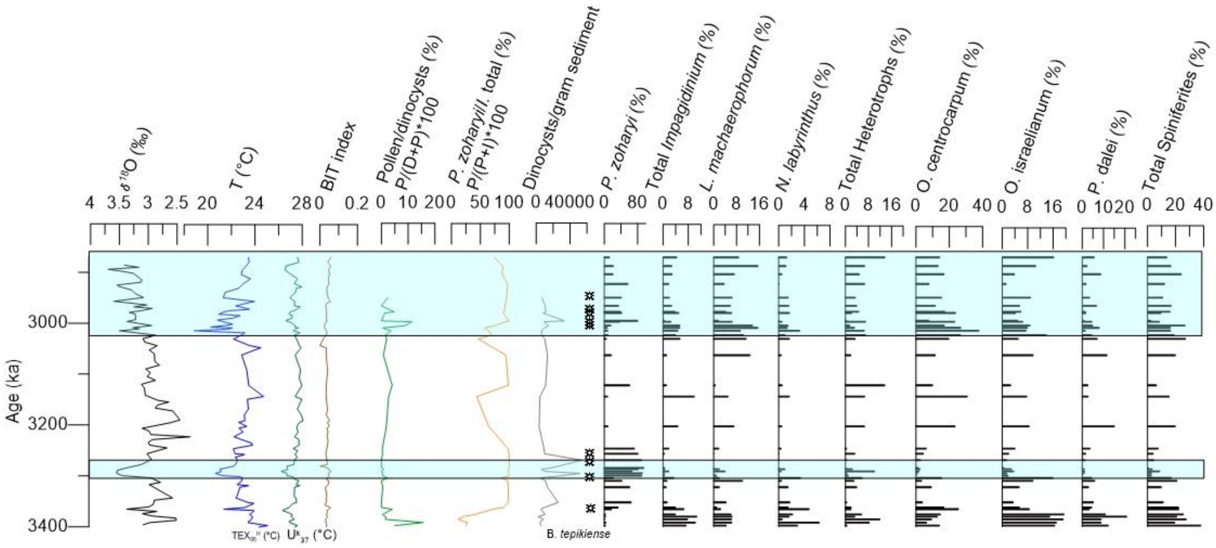

Figure 10: Overview of δ^{18}O, SST, BIT and dinocyst data.

P. zoharyi, O. centrocarpum, O. israelianum, I. spp, L. machaerophorum and *B. tepikiense* have clear environmental preferences and will be taken into account in the discussion. *P. dalei, Spiniferites spp.* and *N. labyrinthus* occur through a wide range of environments and are therefore left out.

4.3.1 Before M2: 3.400-3.312 Ma

First, the assemblage is dominated by *Impagidinium, O. centrocarpum* and *O. israelianum*. *O. centrocarpum* is a cosmopolitan species, occurring in a large range of environments (Zonneveld et al., 2013) but also reaches high abundances when environmental conditions are changing. *O. israelianum* thrives in subtropical to equatorial environments, corresponding with the reconstructed high near-surface temperatures (27.2°C on average) and subsurface temperatures (23.9°C on average). *O. israelianum* also thrives in environments with high upper water salinities and in coastal sites (Zonneveld et al., 2013). Limoges et al. (2014) found an increase of *O. israelianum* at site ODP 625B prior to the onset of the last interglacial maximum (135 kyr). They explained this increase by changes in sea-surface salinity as a result of a northward shift of the ITCZ. Because of this shift, the warmer and salty waters from the Caribbean could move further into the GoM, which also became warmer and saltier (Limoges et al., 2014). Ziegler el al. (2008) also found a relation between the ITCZ and SSTs in the GoM. During a more southern position of the ITCZ, Caribbean waters could not move far north into the GoM, resulting in relatively cold SSTs (Ziegler et al., 2008).

At 3.365 Ma there is a short period with lower temperatures, where near-surface temperatures drop to 26.6°C and subsurface temperatures to 21.4°C. At the same time the dinocyst assemblages change (Fig. X). This change starts with a relative increase of *O. centrocarpum*, which is an indicator of changing environmental conditions. During these colder conditions, the relative abundance of the warm species *O. israelianum* decreased and the cold species *B. tepikiense* (Zonneveld et al., 2013) occurred, although in low abundances. However, as it is a temperate to cold species, living in an environments of -2°C to 26.9°C and not present in the modern day GoM (Zonneveld et al., 2013), its presence points towards a cooling environment. Based on the colder SSTs, the decrease of *O. israelianum* and the occurrence of *B. tepikiense*, warm and salty Caribbean waters likely did not reach far into the GoM from 3.365 Ma to 3.354 Ma.

In the present day GoM, the dinoflagellate assemblage is mostly determined by distance to the coast and water depth. The proximity to the coast can be seen with the ratio between *P. zoharyi* and *Impagidinium spp*, where *P. zoharyi* increases shorewards and is a lagoonal species while *Impagidinium* increases towards deeper waters (Limoges et al., 2013). This trend is also visible towards M2 (Fig. X).

First, *Impagidinium spp*. is dominant over *P. zoharyi*, indicating an open oceanic environment, whereas at 3.365 Ma the conditions start to change and the ratio switches and *P. zoharyi* becomes dominant over *Impagidinium spp* (Fig. 10). During the ratio switch at 3.365 Ma, TEX_{86} and U^{k}_{37} SSTs drop to 21.4°C and 26.6°C respectively, and $\delta^{18}O$ values increase, visible in figure 10. However, sea level dropped maximum 20 meters as is visible in figure 7, which is not enough to create a lagoonal environment at site ODP 625B, as is visible in figure 6. So during the Late Pliocene, the ratio between *Impagidinium spp* and *P. zoharyi* is likely not an indicator for open ocean vs. nearshore environment as it is during the present day (Limoges, et al., 2013). A possible explanation for the occurrence of *P. zoharyi* in an open oceanic environment is hyperstratification (Reichart et al., 2004), as will be explained in 4.2.2.

After this short period of lower SSTs, both the near-surface as the subsurface SSTs increase again (27.3°C and 23.1°C respectively) but the relative abundances of *Impagidinium, O. centrocarpum* and *O. israelianum* remain low, while *P. zoharyi* increases further. So although SSTs increased again, Caribbean waters likely did not propagate as far north into the GoM as before as the dinoflagellate assemblages did not change back to their initial composition.

L. machaerophorum also increases at 3.310 Ma. *L. machaerophorum* is a species that occurs in relatively high abundances near river mouths and when seasonal stratification occurs (Zonneveld et al., 2013). Notably, the high dinocyst over pollen ratio, together with an absence of alkanes and diols at this same time points towards a limited Mississippi influence. However, *L. machaerophorum* can also occur with decreasing upwelling and seasonal stratification. When this happens, there are still nutrients in the upper water column, but the water column becomes stratified (Zonneveld et al., 2013). Hence, stratified conditions as a result of diminished upwelling is a more likely explanation of the occurrence of *L. machaerophorum*.

Hence, the period towards M2 can be seen as a period during which the northern GoM was relatively warm, with near-surface temperatures of 27°C and a high surface water salinity, as indicated by the presence of *O. israelianum*. Those conditions could develop as a result of a northward shift of the ITCZ. Because of this shift, warm and salty Caribbean waters could move into the GoM. However, around 3.365 Ma, both sea surface as subsurface temperatures decrease. During this decrease, *P. zoharyi* starts to become the dominant species, possibly indicating hyperstratification. At 3.361 Ma, temperatures start to increase again, although *P. zoharyi* still remains the dominant species, indicating that Caribbean waters likely did not reach as far north into the GoM as before.

4.3.2 M2: 3.312-3.264 Ma

At 3.303 Ma, the relative abundance of *O. centrocarpum* increases to 16%. *O. centrocarpum* is an opportunist species, which thrives under changing conditions. Its presence at the onset of the M2 indicates that the environmental conditions were changing. At the same time, *O. israelianum* increases to 16%. *O. israelianum* is a species that thrives in waters with a high salinity so a possible explanation is that the northern GoM became even saltier at this time. Before 3.303 Ma, the dinocyst assemblages are already changing, however, only after 3.303 Ma the SSTs start to decrease. At 3.299 Ma the U^{k}_{37} and TEX_{86} have dropped to 26.7°C and 20.6°C respectively. During this SST drop, *P. zoharyi* starts to increase and reaches very high relative abundances, up to 94.8%. Today, *P. zoharyi* reaches high concentrations in warm and shallow marine environments (Limoges et al., 2014). However, as discussed in paragraph 4.1.1, it is unlikely that the sea level dropped enough to create shallow marine environments at the location of Site OPD 625B. High concentrations of *P. zoharyi* were also found in an open ocean, the Arabian Sea, during the Pleistocene (Reichart et al., 2004). There, ongoing evaporation and an interruption in the deep mixing, resulted in very high surface water salinity and the development of a strong pycnocline, causing hyperstratification (Reichart et al., 2004). Although the conditions in the Arabian Sea are very different from the GoM, hyperstratification can explain the presence of *P. zoharyi* in the GoM, which is also an open oceanic environment.

Hyperstratification could also explain the increase of relative abundance of *O. israelianum* and *L. machaerophorum* in the GoM during this time interval. During hyperstratification, the water is very saline. So during the period before the hyperstratification was fully developed, the salinity increased already and the upper water column started to become stratified.

The M2 interval, from 3.305 Ma to 3.285 Ma, starts with slightly decreasing SSTs. The environment starts to change, as indicated by the high relative abundance of O. *centrocarpum*. Most likely the water column conditions started to become more saline and stratified, as indicated by *O. israelianum* and *L. machaerophorum*, when the oceanic environment changed towards hyperstratification during the major drop in SSTs. During those conditions, *P. zoharyi* reached very high relative abundances, which still persisted when SSTs had already changed back to the same values as prior to the M2.

4.3.3 Mid-Piacenzian Warm Period: 3.264-3.023 Ma

After the M2, SSTs rose quickly, and remained stable during the whole mPWP, the near-surface SSTs varied between 27.2°C and 28.1°C. However, *P. zoharyi* still remained the dominant species, even when temperatures had returned to similar levels as before the M2, indicating that (seasonal) hyperstratification still occurred in the northern GoM after the cold period. Around 3.246 Ma, conditions started to change and P. *zoharyi* was only present in small values while *O. centrocarpum*, *Spiniferites spp*. and *O. israelianum* start to increase. The dinoflagellate assemblage looks similar as before the M2 so the warm and salty Caribbean waters likely reached the northern GoM again.

4.3.4 The demise of the mPWP starting with G20: 3.023-2.950 Ma

At 3.023 Ma, there is a sharp drop in subsurface temperatures to 18.8°C and a small drop in near-surface temperatures to 27.2°C during an increase in $\delta^{18}O$ values, the start of G20. The temperature drop was enough for the cold species *B. tepikiense* to occur again. During this period, at 3.015 Ma, *O. centrocarpum* reaches relative abundances of 38%, becoming the most abundant species and indicating changing environmental conditions. When *O. centrocarpum* starts to decline, *L. machaerophorum* increases to 15%, pointing towards increased stratification, possibly as a result of river influence. Close after those higher relative abundances of *L. machaerophorum*, the pollen over dinocyst ratio increases to 11.4%. So both the presence of *L. machaerophorum* and that of pollen points towards river influence. However, both diols and n-alkanes are still below detection limit during this interval at ODP 625B, so it is unlikely that the mouth of the Mississippi became closer to site ODP 625B. Here again, the presence of *L. machaerophorum* can indicate the beginning of hyperstratification conditions.
At 2.994 Ma, there is a drop in both near-surface as subsurface temperatures to 26.7°C and 20.8°C respectively. First O. *centrocarpum* increases and then *P. zoharyi* reaches high values of up to 80% again. After this event, *P. zoharyi* decreases but is still higher than during the period before, around 20-40%. Just as during M2, sea level did not drop enough during these

cold periods for the Mississippi river mouth to become close to site ODP 625B (see figure 6 and 7). So the high abundances of P. *zoharyi* are likely indicating hyperstratification again.

5. Summary and conclusions

Throughout the whole studied interval (3.400-2.950 Ma), there is a lack of terrestrial input, as indicated by the absence of diols, alkanes, pollen and the low BIT index. This points towards an absence of Mississippi river influence. However, at 2.515 Ma, pollen were abundant at ODP site 625B indicating terrestrial influence during the Pleistocene. From this can be concluded that the Mississippi changed its course between 2.950 Ma and 2.515 Ma. Further research is needed to indicate the time period during which the Mississippi started to influence the site location.

During the Late Pliocene, TEX_{86} SSTs were on average 23.4°C while the U^{k}_{37} SSTs were on average 27.3°C. The lower temperatures represented by the TEX_{86} index compared to those based on the U^{k}_{37} can be explained by the different depths in the water column the GDGT's and alkenones on which the SSTs are based are produced. As a result, SSTs based on the TEX_{86} represents 0-200 meter while U^{k}_{37} represents the near-surface temperatures. The fact that U^{k}_{37} is nearly saturated can explain why the record shows less variation than the TEX_{86} record as Uk37 becomes less useful at temperatures above 29°C.

The period towards M2 can be seen as a period during which the northern GoM was warm, with near-surface temperatures of 27°C and high surface water salinities, as indicated by the presence of *O*. *israelianum*. Those conditions could develop as a result of a northward shift of the ITCZ. Because of this shift, the LC was stronger and warm and salty waters of the Caribbean could move far into the GoM.

The M2 is characterized by a temperature drop of 1°C to 2°C and an increase of *O. centrocarpum*, representing changing conditions. Then the conditions started to become more saline and stratified, as indicated by *O*. *israelianum* and *L*. *machaerophorum*. Eventually, during the major drop in SST, the salinity was very high and the pycnocline was very shallow and strong, creating hyperstratification. Because of these conditions, the lagoonal species *P. zoharyi* could occur in the open ocean. *P. zoharyi* reached very high relative abundances, which still persisted when SSTs had already changed back to warm values.

During the following mPWP, conditions eventually changed back to the same conditions as before the M2. So warm and salty Caribbean waters were again transported far into the GoM by the LC. However, there are only a few datapoints used in this study for the mPWP, so another study should focus on this period for a better comparison.

After the mPWP, conditions changed again as indicated by the occurrence of *O. centrocarpum* and a drop in TEX_{86} and U^{k}_{37} SSTs of 0.4°C to 0.5°C. Then again, *P*. *zoharyi* reaches high values, indicating hyperstratification. However, this cold period G20 is less intense than the M2, as temperatures did not drop as much and the relative abundances of *P*. *zoharyi* were not as high as during the M2.

This study highlights the importance of a multiproxy approach as biomarkers or dinocyst alone would have told a very different story.

6. References

Castañeda, I. S., Caley, T., Dupont, L., Kim, J. H., Malaizé, B., & Schouten, S. (2016). Middle to Late Pleistocene vegetation and climate change in subtropical southern East Africa. *Earth and Planetary Science Letters*, *450*, 306-316.

De Schepper, S., Groeneveld, J., Naafs, B. D. A., Van Renterghem, C., Hennissen, J., Head, M. J., ... & Fabian, K. (2013). Northern hemisphere glaciation during the globally warm early late Pliocene. *PloS one*, *8*(12), e81508.

De Vernal, A., & Giroux, L. (1991). Distribution of organic walled microfossils in recent sediments from the Estuary and Gulf of St. Lawrence: some aspects of the organic matter fluxes. *Canadian Journal of Fisheries and Aquatic Sciences*, *113*(189), e199.

Dolan, A. M., Haywood, A. M., Hunter, S. J., Tindall, J. C., Dowsett, H. J., Hill, D. J., & Pickering, S. J. (2015). Modelling the enigmatic late pliocene glacial event—Marine isotope stage m2. *Global and Planetary Change*, *128*, 47-60.

Dowsett, H., Dolan, A., Rowley, D., Pound, M., Salzmann, U., Robinson, M., ... & Haywood, A. (2016). The PRISM4 (mid-Piacenzian) palaeoenvironmental reconstruction. *Climate of the Past Discussions*, *12*, 1519-1538.

Dowsett, H. J., Robinson, M. M., & Foley, K. M. (2009). Pliocene three-dimensional global ocean temperature reconstruction. *Climate of the Past*, *5*(4), 769-783.

Dwyer, G. S., & Chandler, M. A. (2008). Mid-Pliocene sea level and continental ice volume based on coupled benthic Mg/Ca palaeotemperatures and oxygen isotopes. *Philosophical Transactions of the Royal Society A: Mathematical, Physical and Engineering Sciences*, *367*(1886), 157-168.

Eglinton, G., & Calvin, M. (1967). Chemical fossils. *Scientific American*, *216*(1), 32-43.

Eglinton, G., & Hamilton, R. J. (1967). Leaf epicuticular waxes. *Science*, *156*(3780), 1322-1335.

Haywood, A. M., Dowsett, H. J., & Dolan, A. M. (2016). Integrating geological archives and climate models for the mid-Pliocene warm period. *Nature communications*, *7*, 10646.

Hopmans, E. C., Weijers, J. W., Schefuß, E., Herfort, L., Damsté, J. S. S., & Schouten, S. (2004). A novel proxy for terrestrial organic matter in sediments based on branched and isoprenoid tetraether lipids. *Earth and Planetary Science Letters*, *224*(1-2), 107-116.

Huguet, C., Hopmans, E. C., Febo-Ayala, W., Thompson, D. H., Damsté, J. S. S., & Schouten, S. (2006). An improved method to determine the absolute abundance of glycerol dibiphytanyl glycerol tetraether lipids. *Organic Geochemistry*, *37*(9), 1036-1041.

IPCC, 2014: Climate Change 2014: Synthesis Report. Contribution of Working Groups I, II and III to the Fifth Assessment Report of the Intergovernmental Panel on Climate Change [Core Writing Team, R.K. Pachauri and L.A. Meyer (eds.)]. IPCC, Geneva, Switzerland, 151 pp

Kim, J. H., Van der Meer, J., Schouten, S., Helmke, P., Willmott, V., Sangiorgi, F., ... & Damsté, J. S. S. (2010). New indices and calibrations derived from the distribution of crenarchaeal isoprenoid tetraether lipids: Implications for past sea surface temperature reconstructions. *Geochimica et Cosmochimica Acta*, *74*(16), 4639-4654.

Lattaud, J., Dorhout, D., Schulz, H., Castañeda, I. S., Schefuß, E., Sinninghe Damsté, J. S., & Schouten, S. (2017). The C 32 alkane-1, 15-diol as a proxy of late Quaternary riverine input in coastal margins. *Climate of the Past*, *13*(8), 1049-1061.

Lawrence, K. T., & Woodard, S. C. (2017). Past sea surface temperatures as measured by different proxies - A cautionary tale from the late Pliocene. *Paleoceanography*, *32*(3), 318-324.

Limoges, A., Londeix, L., & de Vernal, A. (2013). Organic-walled dinoflagellate cyst distribution in the Gulf of Mexico. *Marine Micropaleontology*, *102*, 51-68.

Limoges, A., de Vernal, A., & Van Nieuwenhove, N. (2014). Long-term hydrological changes in the northeastern Gulf of Mexico (ODP-625B) during the Holocene and late Pleistocene inferred from organic-walled dinoflagellate cysts. *Palaeogeography, palaeoclimatology, palaeoecology*, *414*, 178-191.

Lisiecki, L. E., & Raymo, M. E. (2005). A Pliocene-Pleistocene stack of 57 globally distributed benthic δ18O records. *Paleoceanography*, *20*(1).

Miller, K. G., Wright, J. D., Browning, J. V., Kulpecz, A., Kominz, M., Naish, T. R., ... & Sosdian, S. (2012). High tide of the warm Pliocene: Implications of global sea level for Antarctic deglaciation. *Geology*, *40*(5), 407-410.

Müller, P. J., Kirst, G., Ruhland, G., Von Storch, I., & Rosell-Melé, A. (1998). Calibration of the alkenone paleotemperature index U37K′ based on core-tops from the eastern South Atlantic and the global ocean (60° N-60° S). *Geochimica et Cosmochimica Acta*, *62*(10), 1757-1772.

Naish, T. R., & Wilson, G. S. (2008). Constraints on the amplitude of Mid-Pliocene (3.6–2.4 Ma) eustatic sea-level fluctuations from the New Zealand shallow-marine sediment record. *Philosophical Transactions of the Royal Society A: Mathematical, Physical and Engineering Sciences*, *367*(1886), 169-187.

Nürnberg, D., Ziegler, M., Karas, C., Tiedemann, R., & Schmidt, M. W. (2008). Interacting Loop Current variability and Mississippi River discharge over the past 400 kyr. *Earth and Planetary Science Letters*, *272*(1-2), 278-289.

Pospelova, V., Pedersen, T. F., & de Vernal, A. (2006). Dinoflagellate cysts as indicators of climatic and oceanographic changes during the past 40 kyr in the Santa Barbara Basin, southern California. *Paleoceanography*, *21*(2).

Prahl, F. G., & Wakeham, S. G. (1987). Calibration of unsaturation patterns in long-chain ketone compositions for palaeotemperature assessment. *Nature*, *330*(6146), 367.

Reichart, G. J., Brinkhuis, H., Huiskamp, F., & Zachariasse, W. J. (2004). Hyperstratification following glacial overturning events in the northern Arabian Sea. *Paleoceanography*, *19*(2).

Richey, J. N., & Tierney, J. E. (2016). GDGT and alkenone flux in the northern Gulf of Mexico: Implications for the TEX86 and UK'37 paleothermometers. *Paleoceanography*, *31*(12), 1547-1561.

Reid, P. C., & Harland, R. (1977). Studies of Quaternary dinoflagellate cysts from the North Atlantic. *Contributions of stratigraphic palynology*, *1*, 147-169.

Romanin, M. (2013). Palynological analyses to detect melt water pulses in the Gulf of Mexico during the Early Pleistocene. *Unpublished master thesis*

Sachs J.P., Pahnke K., Smittenberg R. and Zhang Z. (2013) Biomarker Indicators of Past Climate. In: Elias S.A. (ed.) The Encyclopedia of Quaternary Science, vol. 2, pp. 775-782. Amsterdam: Elsevier.

Sachse, D., Billault, I., Bowen, G. J., Chikaraishi, Y., Dawson, T. E., Feakins, S. J., ... & Polissar, P. (2012). Molecular paleohydrology: interpreting the hydrogen-isotopic composition of lipid biomarkers from photosynthesizing organisms. *Annual Review of Earth and Planetary Sciences*, *40*, 221-249.

Salzmann, U., Haywood, A. M., Lunt, D. J., Valdes, P. J., & Hill, D. J. (2008). A new global biome reconstruction and data-model comparison for the Middle Pliocene. *Global Ecology and Biogeography*, *17*(3), 432-447.

Schouten, S., Hopmans, E. C., Schefuß, E., & Damste, J. S. S. (2002). Distributional variations in marine crenarchaeotal membrane lipids: a new tool for reconstructing ancient sea water temperatures?. *Earth and Planetary Science Letters*, *204*(1-2), 265-274.

Seki, O., Foster, G. L., Schmidt, D. N., Mackensen, A., Kawamura, K., & Pancost, R. D. (2010). Alkenone and boron-based Pliocene pCO2 records. *Earth and Planetary Science Letters*, *292*(1-2), 201-211.

Sluijs, A., Pross, J., & Brinkhuis, H. (2005). From greenhouse to icehouse; organic-walled dinoflagellate cysts as paleoenvironmental indicators in the Paleogene. *Earth-Science Reviews*, *68*(3-4), 281-315.

Wall, D., & Dale, B. (1968). Modern dinoflagellate cysts and evolution of the Peridiniales. *Micropaleontology*, *14*(3), 265-304.

Zabeti, N., Bonin, P., Volkman, J. K., Jameson, I. D., Guasco, S., & Rontani, J. F. (2010). Potential alteration of U 37 K′ paleothermometer due to selective degradation of alkenones by marine bacteria isolated from the haptophyte Emiliania huxleyi. *FEMS microbiology ecology*, *73*(1), 83-94.

Ziegler, M., Nürnberg, D., Karas, C., Tiedemann, R., & Lourens, L. J. (2008). Persistent summer expansion of the Atlantic Warm Pool during glacial abrupt cold events. *Nature Geoscience*, *1*(9), 601.

Zonneveld, K. A., Marret, F., Versteegh, G. J., Bogus, K., Bonnet, S., Bouimetarhan, I., ... & Esper, O. (2013). Atlas of modern dinoflagellate cyst distribution based on 2405 data points. *Review of Palaeobotany and Palynology*, *191*, 1-197.

Appendices

Appendix 1: Site ODP625B information

Sample code	*Leg*	*Site*	*Hole*	*Core*	*Sect*	*Half*	*Top (cm)*	*Bottom (cm)*	*MBSF*	*Age (ka)*
GGOM8	100	625	B	16	5	W	77	79	134.1	2928.9
GGOM8.1	100	625	B	16	5	W	87	89	134.2	2931.3
GGOM9	100	625	B	16	5	W	109	111	134.42	2936.7
GGOM9.1	100	625	B	16	5	W	121	124	134.545	2939.6
GGOM10	100	625	B	16	5	W	137	139	134.7	2943.5
GGOM10.2	100	625	B	16	6	W	11	13	134.95	2950.0
GGOM11	100	625	B	16	6	W	43	45	135.27	2957.4
GGOM11.1	100	625	B	16	6	W	56	58	135.4	2960.6
GGOM12	100	625	B	16	6	W	78	80	135.62	2966.0
GGOM12.1	100	625	B	16	6	W	86	88	135.7	2967.9
GGOM13	100	625	B	16	6	W	106	108	135.9	2972.8
GGOM13.1	100	625	B	16	6	W	116	118	136	2975.2
GGOM13.2	100	625	B	16	6	W	126	128	136.1	2977.7
GGOM14	100	625	B	16	6	W	136	138	136.2	2980.1
GGOM14.1	100	625	B	16	6	W	145	147	136.29	2982.3
GGOM14.2	100	625	B	16	CC	W	5	7	136.41	2985.2
GGOM14.3	100	625	B	17	1	W	2	4	136.62	2990.4
GGOM14.4	100	625	B	17	1	W	16	19	136.765	2993.9
GGOM15	100	625	B	17	1	W	23	25	136.83	2995.5
GGOM15.1	100	625	B	17	1	W	36	38	136.96	2997.3
GGOM16	100	625	B	17	1	W	50	52	137.1	3002.1
GGOM16.1	100	625	B	17	1	W	61	63	137.21	3004.8
GGOM16.2	100	625	B	17	1	W	72	74	137.32	3007.4
GGOM17	100	625	B	17	1	W	80	82	137.4	3009.4
GGOM17.1	100	625	B	17	1	W	88	90	137.48	3011.3
GGOM17.2	100	625	B	17	1	W	103	106	137.63	3015.0
GGOM18	100	625	B	17	1	W	111	113	137.71	3019.0
GGOM18.1	100	625	B	17	1	W	120	123	137.8	3023.4
GGOM19	100	625	B	17	1	W	136	138	137.96	3031.4
GGOM19.2	100	625	B	17	2	W	11	13	138.22	3044.3
GGOM20	100	625	B	17	2	W	19	21	138.3	3048.2
GGOM21	100	625	B	17	2	W	48	50	138.59	3062.6
GGOM22	100	625	B	17	2	W	108	110	139.19	3092.4
GGOM23	100	625	B	17	2	W	139	141	139.5	3107.7
GGOM24	100	625	B	17	3	W	17	19	139.79	3122.1
GGOM25	100	625	B	17	3	W	84	86	140.46	3144.1
GGOM26	100	625	B	17	3	W	108	110	140.7	3149.4
GGOM27	100	625	B	17	4	W	17	19	141.3	3168.6
GGOM28	100	625	B	17	4	W	47	49	141.6	3180.3
GGOM29	100	625	B	17	4	W	77	79	141.9	3191.8
GGOM29.1	100	625	B	17	4	W	85	87	141.98	3194.7
GGOM30	100	625	B	17	4	W	107	109	142.2	3202.7
GGOM30.1	100	625	B	17	4	W	117	119	142.3	3206.4

GGOM31	100	625	B	17	4	W	137	139	142.5	3213.7
GGOM31.1	100	625	B	17	5	W	12	14	142.76	3223.1
GGOM31.2	100	625	B	17	5	W	27	30	142.91	3228.6
GGOM32	100	625	B	17	5	W	46	48	143.1	3235.5
GGOM32.1	100	625	B	17	5	W	57	59	143.21	3239.5
GGOM33	100	625	B	17	5	W	76	78	143.4	3246.5
GGOM33.1	100	625	B	17	5	W	87	89	143.51	3250.7
GGOM33.2	100	625	B	17	5	W	102	106	143.66	3256.4
GGOM34	100	625	B	17	5	W	106	108	143.7	3257.9
GGOM34.1	100	625	B	17	5	W	120	122	143.84	3263.2
GGOM35	100	625	B	17	5	W	136	138	144	3269.2
GGOM35.1	100	625	B	17	6	W	18	20	144.23	3278.0
GGOM36	100	625	B	17	6	W	25	27	144.3	3280.6
GGOM36.1	100	625	B	17	6	W	35	38	144.4	3284.4
GGOM36.2	100	625	B	17	6	W	42	44	144.47	3287.0
GGOM37	100	625	B	17	6	W	53	55	144.58	3291.2
GGOM37.1	100	625	B	17	6	W	63	65	144.68	3295.0
GGOM37.2	100	625	B	17	6	W	78	80	144.83	3299.4
GGOM38	100	625	B	17	6	W	85	87	144.9	3301.4
GGOM38.1	100	625	B	17	6	W	93	96	144.98	3303.8
GGOM38.2	100	625	B	14	6	W	108	110	145.13	3308.2
GGOM39	100	625	B	17	6	W	113	115	145.18	3309.6
GGOM39.2	100	625	B	17	6	W	138	141	145.43	3317.0
GGOM40	100	625	B	17	6	W	145	147	145.5	3319.0
GGOM40.1	100	625	B	17	CC	W	5	8	145.61	3322.2
GGOM40.3	100	625	B	18	1	W	45	47	146.25	3340.7
GGOM40.4	100	625	B	18	1	W	53	56	146.33	3343.3
GGOM40.6	100	625	B	18	1	W	83	86	146.63	3352.1
GGOM41	100	625	B	18	1	W	90	92	146.7	3354.2
GGOM42	100	625	B	18	1	W	117	119	146.97	3362.1
GGOM42.1	100	625	B	18	1	W	128	131	147.08	3365.3
GGOM43	100	625	B	18	2	W	0	2	147.3	3371.7
GGOM43.1	100	625	B	18	2	W	14	16	147.44	3375.8
GGOM44	100	625	B	18	2	W	28	30	147.58	3379.9
GGOM44.1	100	625	B	18	2	W	46	49	147.76	3385.2
GGOM45	100	625	B	18	2	W	59	61	147.89	3389.0
GGOM45.1	100	625	B	18	2	W	68	70	147.98	3391.7
GGOM46	100	625	B	18	2	W	88	90	148.18	3397.5
GGOM46.1	100	625	B	18	2	W	97	100	148.28	3400.5

Appendix 2: BIT, U^{k}_{37} SSTs and TEX_{86} SSTs

Sample code	***MBSF***	***Age (ka)***	***BIT***	***SST*** *TEX_{86}*	***SST*** *U^{k}_{37}*
GGOM8	134.1	2928.9	0.040322	22.97683	27.96688
GGOM8.1	134.2	2931.3	0.036432	22.626	27.52226
GGOM9	134.42	2936.7	0.035441	23.86129	27.43452
GGOM9.1	134.545	2939.6	0.037137	21.46853	27.41343
GGOM10	134.7	2943.5	0.033372	23.30944	
GGOM10.2	134.95	2950.0	0.043132	21.30965	26.94873
GGOM11	135.27	2957.4	0.056459	23.98367	27.35729
GGOM11.1	135.4	2960.6	0.037648	23.31343	27.33993
GGOM12	135.62	2966.0	0.031105	22.35	27.34056
GGOM12.1	135.7	2967.9	0.029602	22.75085	27.81797
GGOM13	135.9	2972.8	0.035865	23.55311	27.5186
GGOM13.1	136	2975.2	0.033959	21.9674	27.30275
GGOM13.2	136.1	2977.7	0.034752	21.33986	27.01191
GGOM14	136.2	2980.1	0.035765	21.18168	26.90055
GGOM14.1	136.29	2982.3	0.035568	20.92745	26.8697
GGOM14.2	136.41	2985.2	0.034461	22.74477	27.18015
GGOM14.3	136.62	2990.4	0.033916	22.06959	27.10226
GGOM14.4	136.765	2993.9	0.035337	20.80221	26.68671
GGOM15	136.83	2995.5		23.12614	26.62825
GGOM15.1	136.96	2997.3	0.033042	21.31755	26.92974
GGOM16	137.1	3002.1	0.025033	22.11489	
GGOM16.1	137.21	3004.8	0.025809	21.38312	27.4061
GGOM16.2	137.32	3007.4	0.021849	20.25837	27.37838
GGOM17	137.4	3009.4	0.028324	22.10016	27.68134
GGOM17.1	137.48	3011.3	0.02948	21.75656	27.42659
GGOM17.2	137.63	3015.0	0.032589	18.83144	27.23854
GGOM18	137.71	3019.0	0.038787	23.15366	27.82337
GGOM18.1	137.8	3023.4	0.03284	22.82064	27.30957
GGOM19	137.96	3031.4	0.017028	22.1857	27.5262
GGOM19.2	138.22	3044.3		23.56252	27.75606
GGOM20	138.3	3048.2	0.033317	24.4812	27.89998
GGOM21	138.59	3062.6	0.033786	22.87771	27.39695
GGOM22	139.19	3092.4	0.041335	23.30772	27.85183
GGOM23	139.5	3107.7		24.02303	27.7287
GGOM24	139.79	3122.1	0.033851	23.45941	27.97046
GGOM25	140.46	3144.1	0.033614	24.72345	27.40267
GGOM26	140.7	3149.4	0.033894	23.36003	27.96154
GGOM27	141.3	3168.6	0.040352	23.43068	27.58079
GGOM28	141.6	3180.3	0.034219	23.09795	27.91719
GGOM29	141.9	3191.8	0.052006	23.12823	28.06465
GGOM29.1	141.98	3194.7	0.040153	22.6177	27.77832
GGOM30	142.2	3202.7	0.049451	23.29539	27.53314
GGOM30.1	142.3	3206.4	0.037688	22.63902	27.55159
GGOM31	142.5	3213.7	0.042711	22.98543	27.64705

GGOM31.1	142.76	3223.1	0.03741	22.218	27.35292
GGOM31.2	142.91	3228.6	0.042218	22.85909	27.70684
GGOM32	143.1	3235.5	0.04214	23.69977	27.72331
GGOM32.1	143.21	3239.5	0.039797	23.80139	27.72388
GGOM33	143.4	3246.5	0.036913	22.17415	27.24098
GGOM33.1	143.51	3250.7	0.033494	22.21257	27.6149
GGOM33.2	143.66	3256.4		22.31579	27.41381
GGOM34	143.7	3257.9	0.031326	23.13212	27.41222
GGOM34.1	143.84	3263.2	0.033518	22.33073	27.56616
GGOM35	144	3269.2	0.03859	22.5205	27.3454
GGOM35.1	144.23	3278.0	0.038167	22.32808	27.27692
GGOM36	144.3	3280.6		22.23222	26.71743
GGOM36.1	144.4	3284.4	0.043649	21.53149	26.70312
GGOM36.2	144.47	3287.0	0.043789	21.00946	26.79596
GGOM37	144.58	3291.2	0.060318	21.14355	26.21494
GGOM37.1	144.68	3295.0	0.045155	20.64225	26.70383
GGOM37.2	144.83	3299.4	0.04782	21.23215	26.67271
GGOM38	144.9	3301.4	0.048284	22.71661	27.20018
GGOM38.1	144.98	3303.8	0.038815	22.94743	27.2457
GGOM38.2	145.13	3308.2	0.036913	22.85064	27.4995
GGOM39	145.18	3309.6	0.046787	22.87478	27.69701
GGOM39.2	145.43	3317.0	0.043619	22.47955	27.48586
GGOM40	145.5	3319.0	0.039623	23.47275	27.79748
GGOM40.1	145.61	3322.2	0.028924	22.72577	27.34829
GGOM40.3	146.25	3340.7	0.037119	22.44962	27.31054
GGOM40.4	146.33	3343.3	0.033359	22.37631	27.45824
GGOM40.6	146.63	3352.1	0.034662	23.39689	27.52508
GGOM41	146.7	3354.2	0.029443	23.90619	27.21895
GGOM42	146.97	3362.1	0.056796	23.13607	26.86804
GGOM42.1	147.08	3365.3	0.046753	21.35468	26.55865
GGOM43	147.3	3371.7	0.039389	23.77376	26.77967
GGOM43.1	147.44	3375.8	0.033787	23.53836	27.14155
GGOM44	147.58	3379.9	0.040693	23.78349	27.07217
GGOM44.1	147.76	3385.2	0.030142	23.71385	27.32364
GGOM45	147.89	3389.0	0.031424	23.46917	26.89217
GGOM45.1	147.98	3391.7	0.031956	23.42014	26.95681
GGOM46	148.18	3397.5	0.036278	25.06998	27.59263
GGOM46.1	148.28	3400.5	0.032821	24.31588	27.35082

Appendix 3: Relative abundances dinocysts

GOM code	Depth (mbsf)	Age (ka)	Gram sediment	Achomosphaera	I. aculeatum	I. paradoxum	I. patulum	I. strialatum	Impagidinium spp	Lingulodinium	Melitasphaeridium	O. centrocarpum	O. israeilanum	O. centro short process	P. dalei	Polysphaeridium	S. bentorii	S. mira + S. hyper	S.pachyderma	S. ramosus	Spiniferites spp	Brigantedinium	N. labyrinthus	Pyxidinium	Echinidinium	B. tepikiense	Hystricokolpoma	Total heterotroph	Indet.	Pollen	Bissacates	Lycopodium
GGOM1	131.99	2871.0	5.0	0.0	1.2	3.1	0.0	0.0	0.0	8.7	2.5	14.3	16.1	0.0	5.6	12.4	1.9	7.5	0.0	11.8	0.0	13.7	1.2	0.0	0.0	0.0	0.0	13.7	0.0	0.0	0.0	36.0
GGOM3	132.60	2888.0	5.1	0.0	0.6	1.7	0.0	0.6	0.0	15.5	0.6	13.3	10.5	0.0	2.2	21.5	2.8	9.4	1.7	12.2	0.0	6.6	1.1	0.0	0.0	0.0	0.0	6.6	0.0	0.0	0.0	22.7
GGOM5	133.20	2904.0	5.2	1.4	0.0	1.9	1.0	0.0	0.0	7.2	1.4	16.8	3.8	0.0	8.7	20.7	1.4	9.1	1.4	19.7	0.0	4.8	0.5	0.0	0.0	0.0	0.0	4.8	0.0	0.0	0.0	23.1
GGOM7	133.85	2923.0	5.0	0.0	0.0	0.0	1.8	0.0	0.0	3.6	2.4	7.8	1.2	0.0	1.8	56.6	0.0	6.0	0.0	12.0	0.0	6.6	0.0	0.0	0.0	0.0	0.0	6.6	0.0	0.0	0.0	8.4
GGOM10.2	134.95	2950.0	10.1	0.0	0.0	1.0	1.0	0.0	0.0	6.4	0.0	15.3	8.9	2.5	3.4	40.9	0.5	3.4	0.0	7.4	3.0	3.4	1.5	0.0	0.0	1.5	2.5	3.4	5.4	2.5	50.2	14.3
GGOM12	135.62	2966.0	10.0	0.0	0.4	1.6	0.8	0.0	0.0	5.8	0.4	11.7	5.4	0.0	6.6	34.2	2.7	10.9	1.6	4.7	7.8	2.3	1.6	0.0	1.6	0.0	1.6	3.9	1.2	0.0	1.6	8.9
GGOM13.1	136.00	2977.7	10.6	0.0	0.4	1.3	1.7	0.0	0.4	4.2	0.8	17.2	5.9	3.4	1.3	39.1	0.8	3.4	1.3	6.7	7.1	4.6	0.0	0.0	0.0	0.4	0.4	4.6	2.5	5.0	21.0	8.0

GGOM21	*GGOM19*	*GGOM18.1*	*GGOM17.2*	*GGOM17*	*GGOM16.1*	*GGOM15.1*	*GGOM15*	*GGOM14*
138.59	137.96	137.80	137.63	137.40	137.21	136.96	136.83	136.20
3063.0	3031.0	3023.4	3015.0	3009.4	3004.8	2997.3	2995.5	2980.1
5.1	5.0	10.3	10.1	10.0	10.5	10.1	10.3	10.1
0.0	0.0	0.0	0.0	0.0	0.0	0.0	0.0	0.0
0.4	1.3	0.5	1.4	0.4	0.0	0.0	0.0	0.4
0.4	2.0	1.5	1.9	1.8	4.4	1.5	0.0	0.0
0.4	1.3	1.5	0.9	2.2	0.5	1.0	0.4	4.2
0.0	0.7	0.0	0.0	0.9	0.0	0.0	0.0	0.0
0.0	0.0	0.5	0.5	0.0	0.5	0.0	0.0	0.4
12.7	11.3	10.4	9.3	15.4	13.6	6.4	1.6	6.3
0.0	0.0	0.0	0.0	0.4	0.5	0.0	0.0	0.4
11.6	19.7	26.7	37.9	26.9	17.0	23.3	7.6	23.8
9.7	5.0	13.9	7.5	7.9	8.7	6.4	4.8	4.2
4.1	7.3	0.0	0.0	0.0	1.0	1.0	0.0	0.0
11.6	7.0	4.5	1.4	7.9	4.9	4.5	0.8	1.7
16.8	4.7	8.9	8.4	7.0	15.5	37.1	80.3	41.7
1.9	1.7	0.0	0.0	1.8	2.9	0.5	1.2	0.0
9.3	7.7	5.0	4.7	8.4	3.4	2.5	1.6	3.3
1.5	3.0	4.5	1.4	2.2	0.0	0.0	0.0	2.5
9.0	12.3	10.4	3.7	5.7	6.8	2.0	1.2	4.6
7.5	10.0	4.0	11.2	6.6	17.0	5.9	0.0	2.5
1.9	2.7	4.5	4.2	1.8	1.5	6.9	0.4	1.7
0.4	1.7	1.0	3.3	1.3	1.5	0.5	0.0	1.7
1.1	0.0	0.0	0.0	0.0	0.0	0.0	0.0	0.0
0.0	0.7	2.5	2.3	1.3	0.0	0.0	0.0	0.4
0.0	0.0	0.0	0.0	0.0	0.5	0.5	0.0	0.4
0.0	0.0	0.0	1.9	0.0	0.0	0.5	0.0	0.0
1.9	3.3	6.9	6.5	3.1	1.5	6.9	0.4	2.1
0.0	0.0	5.9	4.7	1.3	2.9	1.5	0.0	0.0
0.7	2.0	1.5	3.7	0.4	9.7	12.9	0.0	1.3
9.7	5.3	29.7	33.2	6.6	12.1	34.7	1.6	20.4
14.2	19.0	14.9	15.0	10.1	6.3	10.4	2.8	11.7

GGOM37	GGOM36.2	GGOM36.1	GGOM35	GGOM33.2	GGOM33	GGOM30	GGOM25	GGOM24
144.58	144.47	144.40	144.00	143.66	143.40	142.20	140.46	139.79
3291.0	3287.0	3284.4	3269.2	3256.4	3246.5	3202.7	3144.1	3122.1
10.1	10.2	10.5	10.0	10.4	10.2	10.2	5.1	5.5
0.0	0.0	0.0	0.0	0.0	0.0	0.0	0.0	0.0
0.4	0.5	0.0	0.0	0.0	0.0	0.5	1.6	0.0
0.4	0.0	0.0	0.0	0.0	1.1	0.9	4.9	0.5
1.1	0.0	0.0	0.0	0.4	0.7	2.8	2.2	0.5
0.0	0.0	0.5	0.0	0.0	0.0	0.0	1.1	0.0
0.0	0.0	0.0	0.0	0.0	0.0	0.5	0.0	0.0
4.0	1.9	0.0	0.0	0.0	1.8	7.0	4.9	0.5
0.0	0.0	0.0	0.4	0.0	0.4	0.9	0.5	0.0
1.8	2.4	1.4	2.7	4.4	6.1	23.5	30.8	9.9
3.6	2.9	0.5	1.3	2.0	4.0	8.5	7.7	2.6
0.0	0.0	0.0	0.0	0.0	0.0	0.0	0.0	0.0
1.1	1.0	0.0	1.3	1.6	3.6	15.0	2.7	2.6
66.5	81.7	94.8	88.9	80.6	71.9	8.5	7.7	60.7
0.0	0.0	0.0	0.0	0.0	0.4	0.5	1.6	0.5
2.2	2.9	2.4	0.0	3.2	2.2	4.7	10.4	1.0
1.1	1.0	0.5	0.9	0.4	2.2	0.5	0.0	0.0
3.6	2.4	0.0	2.7	2.4	3.2	2.8	6.6	3.1
4.0	0.0	0.0	0.9	1.2	1.8	16.0	7.1	2.6
10.1	2.4	0.0	0.4	1.6	0.4	4.2	3.8	1.0
0.4	1.0	0.0	0.0	0.0	0.4	0.5	1.6	0.5
0.0	0.0	0.0	0.0	0.0	0.0	0.5	1.6	1.0
0.0	0.0	0.0	0.0	1.6	0.0	2.3	2.7	12.6
0.0	0.0	0.0	0.4	0.4	0.0	0.0	0.0	0.0
0.0	0.5	0.0	0.0	0.0	0.0	0.5	1.6	0.0
10.1	2.4	0.0	0.4	3.2	0.4	6.6	6.6	13.6
0.0	0.0	0.0	0.0	0.0	0.0	7.0	8.2	0.0
0.0	1.0	0.0	0.0	0.4	0.4	1.9	2.7	4.2
0.0	34.1	6.6	1.8	24.2	8.6	53.1	69.2	48.2
9.4	15.4	5.2	1.8	9.3	10.4	27.2	42.9	15.7

GGOM42.1	*GGOM42*	*GGOM40.6*	*GGOM40.1*	*GGOM39*	*GGOM38.1*	*GGOM37.2*	*GGOM37.1*
147.08	146.97	146.63	145.61	145.18	144.98	144.83	144.68
3365.3	3362.1	3352.1	3322.2	3309.6	3303.8	3299.4	3295.0
10.3	10.1	10.9	10.7	10.2	10.1	10.2	10.2
0.0	0.0	0.0	0.0	0.0	0.0	0.0	0.0
0.0	0.5	0.0	0.5	0.0	0.5	0.0	0.0
5.7	2.9	1.3	0.0	0.0	2.4	0.0	0.5
0.0	0.0	0.0	0.5	1.3	0.0	0.4	0.0
0.9	0.5	0.0	0.0	0.0	0.5	0.0	0.0
0.0	0.0	0.0	0.0	0.0	0.0	0.0	0.0
2.4	1.0	4.3	1.9	10.0	1.9	0.9	0.0
0.0	1.5	0.0	0.0	0.0	0.0	0.0	0.0
25.5	16.7	3.9	9.2	3.3	15.4	0.0	0.9
8.5	5.4	3.4	5.3	9.6	15.9	1.8	1.4
1.9	0.0	0.0	0.0	0.0	0.0	0.0	0.0
3.3	4.4	5.2	2.9	5.9	4.3	0.0	0.9
17.0	32.8	64.4	61.2	41.8	21.6	89.7	91.3
1.9	0.0	2.1	1.5	0.0	2.4	0.0	0.0
4.7	8.8	4.3	3.4	3.8	11.1	3.6	1.8
1.9	0.5	0.9	0.5	5.4	0.5	0.0	0.5
7.5	4.4	3.4	2.9	5.9	9.1	2.7	1.8
10.8	17.2	4.7	4.9	9.6	4.8	0.0	0.5
1.4	2.0	0.4	2.9	1.7	5.3	0.9	0.5
4.7	1.5	1.7	1.5	0.4	3.4	0.0	0.0
0.0	0.0	0.0	0.0	0.0	0.0	0.0	0.0
0.5	0.0	0.0	1.0	1.3	0.5	0.0	0.0
1.4	0.0	0.0	0.0	0.0	0.5	0.0	0.0
0.5	0.5	0.0	0.5	0.4	0.5	0.0	0.0
1.9	2.0	0.4	3.9	2.9	5.8	0.9	0.5
12.7	19.6	0.4	1.5	1.3	0.5	0.0	0.0
4.2	0.0	0.0	0.5	0.0	2.4	0.4	0.5
33.5	26.5	10.7	32.0	3.8	56.7	10.8	9.1
16.0	10.3	3.4	6.8	8.8	17.8	3.1	1.8

GGOM46	*GGOM45.1*	*GGOM44.1*	*GGOM44*	*GGOM43.1*
148.18	147.98	147.76	147.58	147.44
3397.5	3391.7	3385.2	3379.9	3375.8
10.0	10.0	10.4	10.1	10.3
0.0	0.0	0.0	0.0	0.0
1.5	1.0	1.0	2.7	0.4
1.5	6.8	6.2	2.7	3.0
1.0	1.9	0.5	0.5	0.4
2.9	0.0	0.0	2.7	0.0
0.5	0.5	0.0	2.1	0.0
4.4	6.3	6.2	6.4	6.0
0.5	2.9	1.0	0.0	0.4
14.1	6.3	9.3	12.8	14.7
16.5	17.0	19.2	14.9	19.4
0.0	1.5	1.6	0.0	3.0
12.1	8.7	8.8	20.7	10.8
2.4	3.9	1.0	2.7	2.6
0.0	2.4	2.1	1.6	1.7
1.5	9.2	5.2	6.4	6.0
1.9	2.9	15.5	2.1	2.6
1.9	5.3	4.1	7.4	9.9
34.0	8.7	5.7	9.6	11.2
0.0	5.8	2.1	0.0	2.6
2.9	6.3	0.5	1.6	2.2
0.0	0.0	0.0	0.0	0.0
0.5	2.4	9.8	3.2	3.0
0.0	0.0	0.0	0.0	0.0
0.0	0.0	0.0	0.5	0.0
0.5	8.3	11.9	3.2	5.6
18.0	2.4	6.2	8.0	1.7
5.3	18.4	1.6	1.6	0.4
57.8	69.4	9.8	45.7	19.4
16.5	23.3	10.9	39.9	9.1

Appendix 4 absolute abundances

GGOM code	GGOM1	GGOM3	GGOM5	GGOM7	GGOM10.2	GGOM12
Depth (mbsf)	131.99	132.6	133.2	133.85	134.95	135.62
Age (ka)	2871	2888	2904	2923	2950	2966
Gram sediment	5.02	5.13	5.23	4.96	10.09	10.04
Achomosphaera	0.0	0.0	604.1	0.0	0.0	0.0
I. aculeatum	333.3	235.8	0.0	0.0	0.0	420.3
I. paradoxum	833.3	707.3	805.5	0.0	666.6	1681.0
I. patulum	0.0	0.0	402.8	2071.3	666.6	840.5
I. strialatum	0.0	235.8	0.0	0.0	0.0	0.0
Impagidinium spp	0.0	0.0	0.0	0.0	0.0	0.0
Lingulodinium	2333.2	6601.2	3020.6	4142.6	4333.0	6303.9
Melitasphaeridium	666.6	235.8	604.1	2761.7	0.0	420.3
O. centrocarpum	3833.1	5658.1	7048.1	8975.6	10332.6	12607.8
O. israelianum	4333.0	4479.4	1611.0	1380.9	5999.6	5883.7
O. centro short process	0.0	0.0	0.0	0.0	1666.6	0.0
P. dalei	1499.9	943.0	3624.8	2071.3	2333.2	7144.4
Polysphaeridium	3333.1	9194.5	8659.1	64900.3	27664.8	36983.0
S. bentorii	500.0	1178.8	604.1	0.0	333.3	2941.8
S. mira + S. hyper	1999.9	4007.9	3826.1	6904.3	2333.2	11767.3
S.pachyderma	0.0	707.3	604.1	0.0	0.0	1681.0
S. ramosus	3166.4	5186.6	8256.4	13808.6	4999.7	5043.1
Spiniferites spp	0.0	0.0	0.0	0.0	1999.9	8405.2
Brigantedinium	3666.4	2829.1	2013.8	7594.7	2333.2	2521.6
N. labyrinthus	333.3	471.5	201.4	0.0	999.9	1681.0
Pyxidinium	0.0	0.0	0.0	0.0	0.0	0.0
Echinidinium	0.0	0.0	0.0	0.0	0.0	1681.0
B. tepikiense	0.0	0.0	0.0	0.0	999.9	0.0
Hystricokolpoma	0.0	0.0	0.0	0.0	1666.6	1681.0
Total heterotroph	3666.4	2829.1	2013.8	7594.7	2333.2	4202.6
Indet.	0.0	0.0	0.0	0.0	3666.4	1260.8
Pollen	0.0	0.0	0.0	0.0	1666.6	0.0
Bissacates	0.0	0.0	0.0	0.0	33997.7	1681.0
Total dino	26831.5	42671.9	41886.0	114611.1	67662.0	108007.0

GGOM17.2	GGOM17	GGOM16.1	GGOM15.1	GGOM15	GGOM14	GGOM13.1
137.63	137.4	137.21	136.96	136.83	136.2	136
3015	3009.4	3004.8	2997.3	2995.5	2980.1	2977.7
10.10	10.03	10.46	10.09	10.27	10.07	10.63
0.0	0.0	0.0	0.0	0.0	0.0	0.0
906.2	420.3	0.0	0.0	0.0	345.2	508.7
1208.3	1681.0	6691.8	1380.9	0.0	0.0	1526.2
604.1	2101.3	743.5	920.6	1380.9	3452.1	2034.9
0.0	840.5	0.0	0.0	0.0	0.0	0.0
302.1	0.0	743.5	0.0	0.0	345.2	508.7
6041.3	14709.1	20819.1	5983.7	5523.4	5178.2	5087.4
0.0	420.3	743.5	0.0	0.0	345.2	1017.5
24467.1	25635.9	26023.8	21633.4	26236.3	19677.2	20858.2
4833.0	7564.7	13383.7	5983.7	16570.3	3452.1	7122.3
0.0	0.0	1487.1	920.6	0.0	0.0	4069.9
906.2	7564.7	7435.4	4142.6	2761.7	1380.9	1526.2
5437.1	6724.2	23793.2	34521.4	276171.4	34521.4	47312.5
0.0	1681.0	4461.2	460.3	4142.6	0.0	1017.5
3020.6	7985.0	5204.8	2301.4	5523.4	2761.7	4069.9
906.2	2101.3	0.0	0.0	0.0	2071.3	1526.2
2416.5	5463.4	10409.5	1841.1	4142.6	3797.4	8139.8
7249.5	6303.9	26023.8	5523.4	0.0	2071.3	8648.5
2718.6	1681.0	2230.6	6444.0	1380.9	1380.9	5596.1
2114.4	1260.8	2230.6	460.3	0.0	1380.9	0.0
0.0	0.0	0.0	0.0	0.0	0.0	0.0
1510.3	1260.8	0.0	0.0	0.0	345.2	0.0
0.0	0.0	743.5	460.3	0.0	345.2	508.7
1208.3	0.0	0.0	460.3	0.0	0.0	508.7
4228.9	2941.8	2230.6	6444.0	1380.9	1726.1	5596.1
3020.6	1260.8	4461.2	1380.9	0.0	0.0	3052.4
2416.5	420.3	14870.8	11967.4	0.0	1035.6	6104.8
21446.4	6303.9	18588.5	32220.0	5523.4	16915.5	25436.8
64641.4	95399.2	153168.9	92977.7	343833.4	82851.4	121079.4

GGOM33	***GGOM30***	***GGOM25***	***GGOM24***	***GGOM21***	***GGOM19***	***GGOM18.1***
143.4	142.2	140.46	139.79	138.59	137.96	137.8
3246.5	3202.7	3144.1	3122.10744	3063	3031	3023.4
10.18	10.15	5.12	5.50	5.09	5.00	10.28
0.0	0.0	0.0	0.0	0.0	0.0	0.0
0.0	166.7	371.8	0.0	254.4	678.3	322.2
999.9	333.3	1115.3	322.2	254.4	1017.5	966.6
666.6	999.9	495.7	322.2	254.4	678.3	966.6
0.0	0.0	247.8	0.0	0.0	339.2	0.0
0.0	166.7	0.0	0.0	0.0	0.0	322.2
1666.6	2499.8	1115.3	322.2	8648.5	5765.7	6766.2
333.3	333.3	123.9	0.0	0.0	0.0	0.0
5666.3	8332.8	6939.7	6121.8	7885.4	10005.2	17398.8
3666.4	2999.8	1734.9	1611.0	6613.6	2543.7	9021.6
0.0	0.0	0.0	0.0	2798.1	3730.7	0.0
3333.1	5333.0	619.6	1611.0	7885.4	3561.2	2899.8
66662.1	2999.8	1734.9	37375.2	11446.6	2374.1	5799.6
333.3	166.7	371.8	322.2	1271.8	847.9	0.0
1999.9	1666.6	2354.5	644.4	6359.2	3900.3	3222.0
1999.9	166.7	0.0	0.0	1017.5	1526.2	2899.8
2999.8	999.9	1487.1	1933.2	6104.8	6274.4	6766.2
1666.6	5666.3	1611.0	1611.0	5087.4	5087.4	2577.6
333.3	1499.9	867.5	644.4	1271.8	1356.6	2899.8
333.3	166.7	371.8	322.2	254.4	847.9	644.4
0.0	166.7	371.8	644.4	763.1	0.0	0.0
0.0	833.3	619.6	7732.8	0.0	339.2	1611.0
0.0	0.0	0.0	0.0	0.0	0.0	0.0
0.0	166.7	371.8	0.0	0.0	0.0	0.0
333.3	2333.2	1487.1	8377.2	1271.8	1695.8	4510.8
0.0	2499.8	1858.8	0.0	0.0	0.0	3866.4
333.3	666.6	619.6	2577.6	508.7	1017.5	966.6
7999.4	18832.0	15614.3	29642.4	6613.6	2713.3	19332.0
92660.3	35497.6	22554.0	61540.2	68170.7	50873.7	65084.4

GGOM38.1	***GGOM37.2***	***GGOM37.1***	***GGOM37***	***GGOM36.2***	***GGOM36.1***	***GGOM35***	***GGOM33.2***
144.98	144.83	144.68	144.58	144.47	144.4	144	143.66
3303.8	3299.4	3295	813.273	3287	3284.4	3269.2	3256.4
10.12	10.23	10.17	10.09	10.21	10.49	10.04	10.39
0.0	0.0	0.0	0.0	0.0	0.0	0.0	0.0
261.2	0.0	0.0	371.8	302.1	0.0	0.0	0.0
1306.2	0.0	2416.5	371.8	0.0	0.0	0.0	0.0
0.0	1380.9	0.0	1115.3	0.0	0.0	0.0	420.3
261.2	0.0	0.0	0.0	0.0	878.7	0.0	0.0
0.0	0.0	0.0	0.0	0.0	0.0	0.0	0.0
1045.0	2761.7	0.0	4089.5	1208.3	0.0	0.0	0.0
0.0	0.0	0.0	0.0	0.0	0.0	2416.5	0.0
8359.8	0.0	4833.0	1858.8	1510.3	2636.2	14499.0	4622.9
8621.0	5523.4	7249.5	3717.7	1812.4	878.7	7249.5	2101.3
0.0	0.0	0.0	0.0	0.0	0.0	0.0	0.0
2351.2	0.0	4833.0	1115.3	604.1	0.0	7249.5	1681.0
11755.9	276171.4	483300.0	68777.3	51350.6	175745.5	483300.0	84052.2
1306.2	0.0	0.0	0.0	0.0	0.0	0.0	0.0
6008.6	11046.9	9666.0	2230.6	1812.4	4393.6	0.0	3362.1
261.2	0.0	2416.5	1115.3	604.1	878.7	4833.0	420.3
4963.6	8285.1	9666.0	3717.7	1510.3	0.0	14499.0	2521.6
2612.4	0.0	2416.5	4089.5	0.0	0.0	4833.0	1260.8
2873.7	2761.7	2416.5	10409.5	1510.3	0.0	2416.5	1681.0
1828.7	0.0	0.0	371.8	604.1	0.0	0.0	0.0
0.0	0.0	0.0	0.0	0.0	0.0	0.0	0.0
261.2	0.0	0.0	0.0	0.0	0.0	0.0	1681.0
261.2	0.0	0.0	0.0	0.0	0.0	2416.5	420.3
261.2	0.0	0.0	0.0	302.1	0.0	0.0	0.0
3134.9	2761.7	2416.5	10409.5	1510.3	0.0	2416.5	3362.1
261.2	0.0	0.0	0.0	0.0	0.0	0.0	0.0
1306.2	1380.9	2416.5	0.0	604.1	0.0	0.0	420.3
30826.7	33140.6	48330.0	0.0	21446.4	12302.2	9666.0	25215.7
54338.6	307931.1	529213.5	103351.8	62829.0	185411.5	543712.5	104224.7

GGOM44.1	GGOM44	GGOM43.1	GGOM42.1	GGOM42	GGOM40.6	GGOM40.1	GGOM39
147.76	147.58	147.44	147.08	146.97	146.63	145.61	145.18
3385.2	3379.9	3375.8	3365.3	3362.1	3352.1	3322.2	3309.6
10.41	10.11	10.29	10.33	10.14	10.87	10.72	10.19
0.0	0.0	0.0	0.0	0.0	0.0	0.0	0.0
920.6	644.4	460.3	0.0	460.3	0.0	690.4	0.0
5523.4	644.4	3222.0	3411.5	2761.7	3624.8	0.0	0.0
460.3	128.9	460.3	0.0	0.0	0.0	690.4	1380.9
0.0	644.4	0.0	568.6	460.3	0.0	0.0	0.0
0.0	515.5	0.0	0.0	0.0	0.0	0.0	0.0
5523.4	1546.6	6444.0	1421.5	920.6	12082.5	2761.7	11046.9
920.6	0.0	460.3	0.0	1380.9	0.0	0.0	0.0
8285.1	3093.1	15649.7	15351.9	15649.7	10874.3	13118.1	3682.3
17030.6	3608.6	20712.9	5117.3	5063.1	9666.0	7594.7	10586.6
1380.9	0.0	3222.0	1137.2	0.0	0.0	0.0	0.0
7824.9	5026.3	11507.1	1990.1	4142.6	14499.0	4142.6	6444.0
920.6	644.4	2761.7	10234.6	30839.1	181237.5	86994.0	46028.6
1841.1	386.6	1841.1	1137.2	0.0	6041.3	2071.3	0.0
4602.9	1546.6	6444.0	2842.9	8285.1	12082.5	4833.0	4142.6
13808.6	515.5	2761.7	1137.2	460.3	2416.5	690.4	5983.7
3682.3	1804.3	10586.6	4548.7	4142.6	9666.0	4142.6	6444.0
5063.1	2319.8	11967.4	6538.8	16110.0	13290.8	6904.3	10586.6
1841.1	0.0	2761.7	852.9	1841.1	1208.3	4142.6	1841.1
460.3	386.6	2301.4	2842.9	1380.9	4833.0	2071.3	460.3
0.0	0.0	0.0	0.0	0.0	0.0	0.0	0.0
8745.4	773.3	3222.0	284.3	0.0	0.0	1380.9	1380.9
0.0	0.0	0.0	852.9	0.0	0.0	0.0	0.0
0.0	128.9	0.0	284.3	460.3	0.0	690.4	460.3
10586.6	773.3	5983.7	1137.2	1841.1	1208.3	5523.4	3222.0
5523.4	1933.2	1841.1	7675.9	18411.4	1208.3	2071.3	1380.9
1380.9	386.6	460.3	2558.6	0.0	0.0	690.4	0.0
8745.4	11083.7	20712.9	20184.9	24855.4	30206.3	45568.3	4142.6
88835.1	24229.4	106786.3	60270.4	93898.3	281522.3	142228.3	110008.3

GGOM46	*GGOM45.1*
148.18	147.98
3397.5	3391.7
10.00	10.00
0.0	0.0
852.9	402.8
852.9	2819.3
568.6	805.5
1705.8	0.0
284.3	201.4
2558.6	2617.9
284.3	1208.3
8244.5	2617.9
9666.0	7048.1
0.0	604.1
7107.4	3624.8
1421.5	1611.0
0.0	1006.9
852.9	3826.1
1137.2	1208.3
1137.2	2215.1
19900.6	3624.8
0.0	2416.5
1705.8	2617.9
0.0	0.0
284.3	1006.9
0.0	0.0
0.0	0.0
284.3	3423.4
10518.9	1006.9
3127.2	7652.3
33831.0	28796.6
58564.6	41483.3